Cnpy1 is a candidate endoplasmic reticulum chaperone of Vomeronasal type 2 GPCRs.

G V S Devakinandan[1], Nandana Nanda[1#], Abdul Rishad[1#], Syed Dastagir Hussain[1#], Sishir Subedi[2], Adish Dani[1*]

1. Tata Institute of Fundamental Research, Hyderabad, India
2. University of British Columbia, Vancouver, Canada

# equal contribution

* Correspondence: adishd@tifrh.res.in

Abstract

Mouse vomeronasal sensory neurons are continuously generated from stem cells and differentiate to express V1R or V2R G-protein coupled receptors (GPCRs), along with their respective Gαi2 or Gαo G-protein subunits. We have previously reported that Gαo-type neurons exhibit elevated expression of endoplasmic reticulum (ER) chaperones and a distinctive hypertrophic, gyroid ER architecture. Here we identify full-length mouse *Cnpy1* with its expression and localization exclusive to the ER of Gαo neurons. *Cnpy1* deletion resulted in mice that were deficient in Gαo neuronal activation upon exposure to vomeronasal stimuli and a marked reduction in male-male aggressive behavior. In Cnpy1$^{-/-}$ mice, Gαo neuron develop normally till birth, but undergo selective, progressive apoptosis during postnatal development, despite normal trafficking of V2R GPCRs to dendritic tips. Immunoprecipitation and mass spectrometry revealed that Cnpy1 associates with V2R GPCRs and other ER chaperones. Together, these findings identify Cnpy1 as a component of an ER chaperone complex essential for Gαo neuron signaling and survival.

Introduction

Animals depend on a highly diversified chemosensory system to sense their environment, seek food as well as social and inter-species interactions. The vomeronasal or accessory olfactory system, comprised of a peripheral vomeronasal organ (VNO) specializes in detection of pheromones, kairomones and such chemo-signals that elicit innate stereotyped behaviors. Several vertebrates, including rodents, have evolved an elaborate VNO molecular organization, with major classes of G-protein coupled receptor (GPCR) families - vomeronasal type-1 (V1R), type-2 (V2R), or formyl-peptide receptors (FPR) (Liberles, 2014) being expressed in spatially segregated sensory neurons within the neuroepithelium, along with the G-protein subunits, Gαi2 or Gαo. VSNs arising from a regenerating stem cell population, differentiate and migrate within the neuroepithelium to take on the identities of Gαi2 expressing V1R, or Gαo expressing V2R, neuronal subtypes. During this process, VSNs transition through distinct stages of progenitor, immature and mature cells, with choreography of cell autonomous and non-cell autonomous differentiation factors. Thus, in addition to serving as an important model system to understand the neurobiology of innate behaviors, the VNO is also a model to study neuronal development and diversification, a process that occurs throughout the lifespan of the organism.

While few ligands that activate V1R or V2R expressing neurons have been identified by calcium or immediate early gene activation studies (Chamero *et al*, 2007; Isogai *et al*, 2011; Kimoto *et al*, 2005; Lee *et al*, 2019) the downstream signaling and cell biology of Gαi2, Gαo neurons remain poorly understood. One of the hurdles has been the inability to reconstitute functional expression and signaling of VRs in heterologous cells, due to GPCR misfolding and retention inside the endoplasmic reticulum (ER), a feature shared with olfactory receptors (OR). Given that OR, V1R, V2R GPCRs are evolutionarily distinct, their expression, maturation, signaling and cell biology may necessitate neurons expressing these GPCRs to diversify in their cellular and molecular components, while sharing certain features. Indeed, earlier studies have identified genes such as *H2-Mv* that are selectively co-expressed with V2Rs and may play a role in receptor function (Ishii & Mombaerts, 2011; Loconto *et al*, 2003). Several examples exist of specific factors, including ER chaperones that are required for the maturation and targeting of sensory GPCRs. The protein ODR-4, is required for ciliary localization of ORs in C.elegans (Dwyer *et al*, 1998), chaperones NinaA,

57 Calnexin and XPORT are essential for Drosophila Rhodopsin GPCR maturation (Baker *et*
58 *al*, 1994; Rosenbaum *et al*, 2011; Rosenbaum *et al*, 2006), receptor transporting proteins,
59 RTP1 and RTP2 aid expression of mammalian ORs (Saito *et al*, 2004) and a VNO specific
60 calreticulin variant, Calr4, has been shown to promote the maturation of V2Rs upon their
61 expression in heterologous cells (Dey & Matsunami, 2011). Chaperoning of ORs and VRs
62 is important for their proper targeting, but also for the survival of the sensory neuron (Sharma
63 *et al*, 2017).
64
65 In our earlier study, performing comparative transcriptomics of V1R expressing Gαi2 and
66 V2R expressing Gαo neurons, we observed that mature Gαo neurons differ by significantly
67 upregulating the expression of genes and proteins whose functions are associated with the
68 endoplasmic reticulum (ER). Furthermore, Gαo neurons adopt a highly hypertrophic ER
69 membrane organization, characterized by a cubic or gyroid membrane ultrastructure. These
70 results suggest a fundamental cell biological divergence of Gαo neurons and prompted us
71 to investigate the role of certain Gαo neuron specific upregulated genes. Here, we identify
72 Cnpy1 as a VNO neuron specific protein, that is exclusively expressed in Gαo-VSNs and
73 localized to the ER. The molecular and functional characterization of Cnpy1, including its
74 absence, highlights the unexpected role of a specialized ER proteins in Gαo that maybe
75 important for V2R GPCRs and neuronal signaling, survival.

Results

Expression of *Cnpy1* in the VNO.

In our recent study, we performed single cell transcriptomics of the mouse VNO and compared transcriptomes of Gαi2 with Gαo expressing neurons (Devakinandan *et al*, 2024). This analysis resulted in the identification of several genes that are selectively upregulated in Gαo neurons. Amongst the Gαo enriched genes, we investigated Canopy1 (*Cnpy1*) in depth to understand its function. From our single cell RNA sequencing data, *Cnpy1* expression is restricted to immature and mature Gαo neurons, with no expression in Gαi2 neurons (**Figure 1A, 1B**).

Cnpy1, first described in zebrafish (Hirate & Okamoto, 2006), belongs to the saposin-like family of proteins. Mammalian CNPY family members, Cnpy2-Cnpy5, homologs of Cnpy1, contain a characteristic six-cysteine saposin like protein (SAPLIP) domain (Schildknegt *et al*, 2019; Sowa *et al*, 2021). However, mouse *Cnpy1* in Ensembl (ENSMUSG00000044681) or NCBI (Gene ID: 26963) databases contains only 4 cysteines, lacking the complete SAPLIP domain and is considered to be a truncated protein with no function attributed as yet. In order to confirm if mouse VNO expresses the truncated version of *Cnpy1*, we used raw (bulk) RNAseq data of VNO (Santoro & Jakob, 2018) and assembled the transcriptome. Interestingly, we found that VNO expresses a *Cnpy1* transcript that contains an additional upstream exon. Translation of the assembled open reading frame indicates that the upstream translation start site from this additional exon contributes a putative signal sequence (1-23 amino acids) predicted by SignalP 6.0 (Teufel *et al*, 2022) (**Figure S1A**), as well as 2 cysteines that complete the SAPLIP domain (**Figure 1C**). Multiple sequence alignment of full length Cnpy1 protein sequence (Cnpy1-FL) with other mouse Cnpy proteins shows the conservation of six-cysteine signature (**Figure 1D**), indicating Cnpy1 may form a functional protein in the VNO.

Cnpy1 is a Gαo neuron specific ER protein.

We reasoned that additional exon of Cnpy1 consisting of an upstream translation start site and a signal sequence was not detected earlier because it may be only expressed in VNO and often VNO genes are poorly annotated in gene expression databases. To confirm if full

length *Cnpy1* expression is specific to VNO we made cDNA from several adult mouse tissues and used these as templates for PCR-based detection. We amplified a region of the exon1-exon2 and exon2-exon3 of Cnpy1-FL. The tissue panel RT-PCR revealed that expression of *Cnpy1* mRNA is restricted mainly to VNO with a faint band observed in the main olfactory epithelium (MOE) (**Figure 2A**). To localize *Cnpy1* expression to olfactory regions, we performed RNA *in-situ* hybridization (RNA-ISH) with a Cnpy1 anti-sense ribo-probe on sections of the VNO, MOE and accessory olfactory bulb (AOB) (**Figure 2B-D**). This experiment confirmed that *Cnpy1* mRNA is restricted to sensory neurons of the VNO and MOE, with no expression in AOB.

Next, to test whether Cnpy1 protein follows the same pattern as its mRNA expression and to study its function, we generated a custom peptide antibody specific to Cnpy1. Immunolabeling of tissue sections revealed a localization pattern similar to Cnpy1 mRNA in the basal zone (**Figure 2E**). Interestingly, we did not see any Cnpy1 protein in the MOE (**Figure 2F**), even though small amount of transcript was detected, indicating the possibility of post-transcriptional regulation of Cnpy1 expression. Western blot analysis of Cnpy1 from VNO and MOE tissue lysates further validated this result, showing a robust band in VNO but absence in MOE (**Figure 2G**). From our single cell transcriptomics data (**Figure 1A, 1B**) and from RNA-ISH (**Figure 2B**) *Cnpy1* expression appeared to be restricted to basal/ Gαo neurons. To confirm if Cnpy1 is exclusive to Gαo neurons, we immunolabeled VNO sections using anti-Cnpy1 together with anti-Gαo or anti-Nsg1 (marker for Gαi2 neurons) along with the antibody against ER retention sequence - SEKDEL, that preferentially marks the cell bodies of Gαo neurons (**Figure S1C, S1D**), (Devakinandan *et al.*, 2024). This showed that Cnpy1 expression is restricted to Gαo neurons (**Figure S1B**) with no labeling in Gαi2 neurons (**Figure S1C**).

Cnpy homologs have been shown to be resident in the ER and function as chaperones of various membrane receptors such as Toll-like receptors and immunoglobulins (Hirate & Okamoto, 2006; Hong *et al*, 2017a; Konno *et al*, 2006; Schildknegt *et al.*, 2019; Shibata *et al*, 2012; Shimizu *et al*, 2009; van Anken *et al*, 2009; Wakabayashi *et al*, 2006). We hypothesized that Cnpy1 is also an ER resident protein and a putative ER chaperone. To identify the subcellular localization of Cnpy1, we co-labelled VNO sections with anti-Cnpy1

140 and anti-Protein Disulphide Isomerase (PDI), a known ER resident chaperone. High
141 resolution confocal microscopy showed that Cnpy1 is co-localized with PDI in the ER of Gαo
142 neurons (**Figure 2H**), indicating that similar to other Cnpy homologs, mouse Cnpy1 is also
143 likely to function in the ER of Gαo VSNs. Further, we cloned Cnpy1 with a N-terminal myc
144 tag after the start codon, or C-terminal myc before it's stop codon, expressed the tagged
145 Cnpy1 proteins via transient transfection in HEK293 cells followed by detection of the
146 expressed protein using anti-Cnpy1 or anti-myc tag antibodies. myc-Cnpy1 could only be
147 detected with anti-Cnpy1, but not with anti-myc (**Figure S2A**), indicating that the N-terminal
148 tag is cleaved off as a result of signal peptide cleavage, whereas C-terminal tagged (Cnpy1-
149 myc) could be detected with both anti-Cnpy1 and anti-myc (**Figure S2B**). Cnpy1 was also
150 observed to be localized to the ER in HEK293 cells (**Figure S2C**), similar to earlier studies
151 that reported the localization of cloned Cnpy2-Cnpy5 to the ER in mammalian cell lines.
152 Interestingly, mouse Cnpy1 C-terminal lacks a KDEL-type ER retrieval sequence, indicating
153 that its ER retention may involve some other motif or mechanism.
154
155 **Loss of Cnpy1 leads to reduction of V2R expressing Gαo neurons.**
156 After confirming that Cnpy1 is an ER protein, we took a loss of function approach to identify
157 the role of Cnpy1 in Gαo neurons. Crispr-Cas9 mediated targeting resulted in a 99 base pair
158 deletion leading to a non-functional form of Cnpy1 protein to generate a Cnpy1-knockout
159 (Cnpy1$^{-/-}$) mouse model (**Figure 3A**). Cnpy1$^{-/-}$ mice did not show any developmental
160 abnormalities, nor any obvious breeding problems and could be maintained as a
161 homozygous knockout line. VNOs collected from Cnpy1$^{-/-}$ mice showed a complete absence
162 of Cnpy1 protein, as characterized by western blot from lysate and immunolabeling of VNO
163 sections (**Figure 3B, 3C**). To identify the effect of loss of Cnpy1, we performed RNA
164 sequencing (RNAseq) of VNO from three replicates each of Cnpy1$^{+/+}$ and Cnpy1$^{-/-}$ littermate
165 mice, at postnatal day 60 age (p60). We identified 111 genes differentially expressed
166 between Cnpy1$^{-/-}$ and Cnpy1$^{+/+}$ with adjusted p-value less than 0.01 and absolute fold
167 change of 1.5. Of these, 84 genes are downregulated and 27 are upregulated in Cnpy1$^{-/-}$
168 compared to Cnpy1$^{+/+}$ (**Figure 3D, Supplementary Table 1**). Among downregulated genes,
169 the major group that stood out is type-2 vomeronasal receptor genes (V2Rs) with about 66
170 V2R genes. This constitutes almost 50% of total V2Rs annotated from the mouse genome.
171 To validate the RNAseq results, we performed qPCR using gene specific TaqMan probes

172 against some of the V2Rs (Vmn2r65, 54, 53, 24, 112, 110, 116, 42, 2r1) and observed their
173 downregulation in Cnpy1$^{-/-}$ compared to Cnpy1$^{+/+}$ VNO (**Figure S3**). Of the 6 V2Rs observed
174 to be upregulated in RNAseq (**Figure 3D**), Vmn2r72 upregulation was also validated by
175 qPCR assay (**Figure S3**). Based on their sequence homology, V2Rs are classified into
176 families A, B, C, D. Members of the A,B,D families largely follow the one-neuron-one-
177 receptor rule, whereas family-C V2Rs are broadly expressed across Gαo neurons, where
178 they are co-expressed with an ABD V2R per cell (Ishii & Mombaerts, 2011; Silvotti *et al*,
179 2007; Young & Trask, 2007). We observed that downregulated V2Rs from **Figure 3D** were
180 dispersed across the family tree, with representation across all families (**Figure S4**). These
181 data indicate that the loss of Cnpy1 significantly impacts specific V2Rs across all families,
182 as seen at the bulk RNA level.
183
184 Next, we sought to investigate V2R downregulation at the protein level in individual neurons
185 using immunohistochemistry. Using custom generated anti-Vmn2r65, anti-Vmn2r111/112
186 antibodies, and anti-pan family-D (Vmn2r53-56) (Silvotti *et al*, 2011), we performed
187 immunolabeling on VNO sections from p60 Cnpy1$^{-/-}$, Cnpy1$^{+/+}$ littermate mice and counted
188 the number of neurons expressing that V2R per section. We also crossed a mouse line that
189 co-expresses GFP in Vmn2r26 expressing neurons (*Vmn2r26-IRES-tauGFP*, also termed
190 V2r1b-IRES-tauGFP) (Del Punta *et al*, 2002), with Cnpy1$^{-/-}$ to count Vmn2r26 neurons in the
191 absence of Cnpy1. These V2Rs (Vmn2r65, family-D, Vmn2r26-GFP, Vmn2r111/112)
192 representing multiple families, showed almost no labeling in Cnpy1$^{-/-}$ compared to Cnpy1$^{+/+}$
193 VNOs (**Figure 3E**), indicating the complete absence of neurons expressing these V2Rs.
194 Lack of V2R expressing cells in Cnpy1$^{-/-}$ indicates that the reduction of receptor mRNA levels
195 seen with bulk RNA seq (**Figure 3D**) is a consequence of reduced cell numbers expressing
196 those receptors rather than attenuated expression at an individual neuron level.
197
198 We asked whether the absence of multiple V2R expressing neurons in Cnpy1$^{-/-}$ VNO results
199 in a reduction in the total number of Gαo neurons. To address this question, we
200 immunolabeled VNO sections with anti-Nsg1 and anti-Gαo antibodies, markers of the
201 apical/basal zone (**Figure S1B**) VSNs respectively. Quantification of the demarcated area
202 in at least 50 sections each from 3 replicates of p60 Cnpy1$^{-/-}$ and Cnpy1$^{+/+}$ littermate mouse
203 VNOs revealed a 35.4% reduction in mean Gαo /basal zone area (**Figure 4A**). Concomitant

204 with a reduction of Gαo neurons, the total sensory epithelium area also showed a reduction
205 in Cnpy1$^{-/-}$ mouse VNOs. Apical or basal VSNs project axons to respective segregated
206 glomerular regions of the AOB. Quantification of the glomerular region area from sagittal
207 sections of the AOB marked by Banderiraea Simplicifolia (BS)-Lectin (Salazar & Sanchez
208 Quinteiro, 2003) and negatively labeled by anti-Gαi2 also revealed a specific reduction in
209 the basal zone region (**Figure 4B**). These data demonstrate that in the absence of Cnpy1,
210 multiple V2R expressing neurons are lost, resulting in a substantial reduction in the Gαo
211 neuroepithelium zone. Thus, the downregulation of almost 50% V2R genes seen in Cnpy1^{-}
212 $^{/-}$ RNAseq data (Figure 3D), could be attributed to the loss of these neurons.
213
214 **Loss of Cnpy1 leads to death of specific Gαo VSNs.**
215 Since we observed a substantial loss of V2R expressing Gαo VSNs in p60 Cnpy1$^{-/-}$ mice,
216 we asked whether these neurons were missing at birth of the animal or are lost later during
217 postnatal development. We counted the numbers of V2R labeled VSNs, (shown in **Figure**
218 **3E**) in sections from mice with and without Cnpy1 at different ages. At age p7, V2R
219 expressing neurons were present in Cnpy1$^{-/-}$ and their numbers comparable with Cnpy1$^{+/+}$.
220 However, by p15 there was a clear reduction of these V2R expressing neurons in Cnpy1$^{-/-}$
221 VNOs that persisted into later ages (**Figure 5A-C, Figure S5A**). This indicates that VSN
222 numbers are normal at birth and decrease during postnatal development. To understand
223 how neurons are being lost, we labelled VNO sections from Cnpy1$^{-/-}$ and Cnpy1$^{+/+}$ mice
224 across postnatal ages with an antibody against cleaved caspase 3 (CC3), a marker for
225 apoptotic neurons (Brann & Firestein, 2010) along with anti-SEKDEL, a marker for Gαo
226 neurons. (**Figure 5D, Figure S1B**). This allowed us to quantify CC3 positive cells within Gαo
227 zone and entire neuroepithelium at each postnatal age. The total number of CC3+ cells
228 showed a significant increase in p15 Cnpy1$^{-/-}$ VNOs compared to Cnpy1$^{+/+}$ controls (**Figure**
229 **5E**). CC3+ cell numbers within Gαo zone (**Figure S5B**) and normalizing these to a declining
230 postnatal Gαo zone in Cnpy1$^{-/-}$ VNOs (**Figure 5F**) show consistently elevated levels p15
231 onwards, compared to age matched Cnpy1$^{+/+}$ VNOs (**Figure 5G**). Immunolabeling of p15
232 Cnpy1$^{-/-}$ sections with anti-CC3 and anti-OMP, confirmed that the elevated number of
233 apoptotic cells in Cnpy1$^{-/-}$ Gαo zone were OMP labelled mature neurons (**Figure S5C**).
234 Further, VNO sections from p60 Cnpy1$^{-/-}$ co-labelled with anti-OMP, anti-Gαo confirmed that
235 residual Gαo neurons in the neuroepithelium of Cnpy1$^{-/-}$ mice were OMP positive, indicating

236 that absence of Cnpy1 does not result in a developmental block prior to mature neuron stage
237 (**Figure S5D**), as seen in the VNOs from mice lacking the transcription factor, ATF5 (Nakano
238 *et al*, 2016).
239 Collectively, these data show that V2R expressing mature VSNs are lost due to apoptotic
240 cell death during early postnatal development after Gαo fate specification in Cnpy1$^{-/-}$ VNO.
241
242 One of the hallmarks of olfactory and vomeronasal neurons, is their continuous regeneration
243 from a stem cell population, which in case of VSNs leads to a developmental transition and
244 cell fate bifurcation via an immature Gαi2 or Gαo state to respective mature neurons
245 (Katreddi *et al*, 2022). To address whether there is a change in the rate of neurogenesis
246 triggered due to loss of Gαo neurons, we labelled VNO sections for Ki67, a marker of cell
247 proliferation (Ohta & Ichimura, 2000). Quantification of Ki67 positive cells revealed a marked
248 increase in p15 Cnpy1$^{-/-}$ mouse VNOs (**Figure 5H**), indicating a consistent and
249 compensatory neurogenesis accompanying the VSN loss due to cell death. Collectively
250 these data indicate that the absence of Cnpy1 results in a loss of dV2R neurons due to cell
251 death during postnatal development that is likely to be sensed and compensated to some
252 extent by enhanced neurogenesis.
253
254 **Cnpy1 interacts with V2Rs and other ER chaperones.**
255 Our next step was to understand the molecular function of Cnpy1 in Gαo neurons. Cnpy1
256 localization to the ER, the function of homologous Cnpy proteins as ER chaperones, and
257 the loss of several V2R expressing VSNs in Cnpy1$^{-/-}$ mice, lead us to ask whether Cnpy1
258 directly interacts with V2Rs, acting as a specific chaperone. To test this, we
259 immunoprecipitated Cnpy1 from lysate of C57BL/6J (B6) VNOs using anti-Cnpy1 antibody
260 ($IP_{Cnpy1:B6}$). As controls, we performed IP from Cnpy1$^{-/-}$ VNO lysate ($IP_{Cnpy1:KO}$) as well as an
261 IP using normal IgG from B6 VNO lysate ($IP_{IgG:B6}$). The protein eluates form all IP samples
262 were fragmented to peptides using trypsin and labeled with TMT. We pooled TMT labelled
263 samples and performed fractionation followed by liquid chromatography-quantitative mass
264 spectrometry to identify the co-immunoprecipitating interacting partners of Cnpy1. Proteins
265 in $IP_{Cnpy1:KO}$ and $IP_{IgG:B6}$ serve as negative controls to identify non-specific interactions.
266 Therefore, we considered common enriched hits based on absolute foldchange more than
267 2, calculated from [$IP_{Cnpy1:B6}$ vs $IP_{Cnpy1:KO}$] and [$IP_{Cnpy1:B6}$ vs $IP_{IgG:B6}$] as true interacting

268 partners of Cnpy1. With this process, we identified 27 specific interacting partners: 13 V2Rs,
269 5 ER chaperones and 9 other proteins of various functions (**Figure 6**, **Supplementary Table**
270 **2**). Due to high sequence homology, the identification of specific V2Rs via MS is likely to be
271 an underestimate, because only unique trypsin cleaved peptides are mapped to V2R
272 sequences. The interaction of Cnpy1 with V2Rs and other ER chaperones indicates that it
273 is a putative V2R specific chaperone that might function along with other chaperones for the
274 proper folding of V2Rs in the ER of Gαo VSNs.
275
276 **Neuronal activation is significantly reduced, but V2R export is unaffected in Cnpy1$^{-/-}$**
277 **VSNs.**
278 To investigate whether V2Rs are exported out of the ER of VSNs in the absence of Cnpy1,
279 we imaged immunolabeled Vmn2r65 (**Figure 3E**) towards the lumen of the vomeronasal
280 sensory epithelium, where VSNs project their dendritic tips. Since Vmn2r65 expressing
281 VSNs are mostly lost by p30 age, we used VNO sections from p15 Cnpy1$^{+/+}$ and Cnpy1$^{-/-}$
282 mice, where Vmn2r65 VSNs are still detected in Cnpy1$^{-/-}$ mice, although with reduced
283 numbers (**Figure 5A**). We observed an equivalent amount of anti-Vmn2r65 signal in Cnpy1^{-}
284 $^{/-}$ as well as Cnpy1$^{+/+}$ dendritic tips (**Figure 7A, 7B**), indicating that post-ER export of V2Rs
285 along the secretory pathway and their targeting is likely to be not defective due to the
286 absence of Cnpy1. Furthermore, we reasoned that if there was a build-up of misfolded V2R
287 GPCRs in Cnpy1$^{-/-}$ VSNs, it should result in an unfolded protein response (UPR), which can
288 be measured using X-box binding protein-1 (*Xbp1*) splicing. PCR amplification of a stretch
289 of *Xbp1* from p14 Cnpy1$^{-/-}$ and Cnpy1$^{+/+}$ VNO cDNA did not reveal elevated *Xbp1* splicing
290 (**Figure 7C**), further confirming the lack of UPR activation in Cnpy1$^{-/-}$ VSNs. As V2R GPCRs
291 are known to be involved in the process of targeting axonal projections to the AOB (Belluscio
292 *et al*, 1999; Rodriguez *et al*, 1999), we also investigated glomerular targeting in Vmn2r26-
293 GFP;Cnpy1$^{-/-}$ p7 mice, when Vmn2r26-GFP neurons can still be detected. GFP labeled
294 axons still coalesce towards the posterior AOB (**Figure 7D**). This indicates that during early
295 postnatal age, the gross anatomical wiring of V2R expressing VSNs to the AOB is not altered
296 in Cnpy1$^{-/-}$, although finer defects in glomerular formation may exist. Collectively, these data
297 rule out V2R protein export from the ER as a mechanism for cell death in Cnpy1$^{-/-}$ Gαo
298 VSNs.
299

300 We next investigated whether VSN activation, downstream of V2R GPCR signaling was
301 affected. Cnpy1$^{-/-}$ and Cnpy1$^{+/+}$ p60 littermate mice were exposed to rat bedding, a source
302 of predator kairomones or opposite sex bedding as a source of pheromones. Both stimuli
303 were shown to be complex sources of ligands for VSNs, and their activation can be
304 measured by immunolabeling VNO sections with an antibody to phosphorylated S6
305 ribosome subunit (pS6) (Silvotti *et al*, 2018). We immunolabeled VNO sections from mice
306 exposed to these stimuli with anti-pS6 and anti-SEKDEL (to mark Gαo zone) and quantified
307 the number of pS6 labeled neurons per section (**Figure 8A-8D**). In case of both stimuli,
308 Cnpy1$^{-/-}$ VNOs showed a clear reduction in the number of activated neurons within Gαo zone
309 compared to Cnpy1$^{+/+}$. These data indicate that despite loss of Gαo neurons in p60 Cnpy1^{-}
310 $^{/-}$ mice due to cell death, the persisting neurons, show significantly reduced activation by
311 ligands. Interestingly, there was a small but significant increase in pS6 cells outside the Gαo
312 zone, which matches with a slight increase in Gαi2 zone we observed earlier (**Figure 4A**),
313 pointing to the possibility of a compensatory increase in the number of Gαi2 neurons in
314 Cnpy1$^{-/-}$ neuroepithelium.
315
316 One of the behavioral consequences of loss of Gαo VSN activation is reduced male-male
317 aggression in a classical resident-intruder paradigm (Chamero *et al*, 2011). Hence, we
318 exposed littermate resident male mice at p60 age to castrated male mice swabbed with male
319 mouse urine. Cnpy1$^{+/+}$ and Cnpy1$^{+/-}$ mice reacted with aggressive behaviors towards the
320 intruder male, while Cnpy1$^{-/-}$ males showed markedly reduced aggressive behaviors towards
321 intruders (**Figure 8E-G**). Collectively, these data indicate that loss of Cnpy1 impairs
322 activation of Gαo VSNs by chemical cues, producing deficits in behaviors normally mediated
323 by this neuronal population.
324
325 **Discussion:**
326 In this study, we identify mouse Cnpy1 as a VNO specific protein, with its expression
327 restricted to the Gαo subtype of sensory neurons. Compared to other Cnpy homologs,
328 mammalian Cnpy1 has remained enigmatic because of an incomplete SAPLIP domain. The
329 novel Cnpy1 transcript we identified in the mouse VNO, includes an additional upstream
330 exon with a new translation start site, that completes full-length Cnpy1 protein by contributing
331 two additional cysteines and a signal peptide. Mapping trypsin digested peptides from our

332 Cnpy1 IP-proteomics, gave additional confidence to the predicted protein sequence (**Figure**
333 **S6**). *Cnpy1* was first described and cloned from zebrafish, where its expression during
334 embryonic development was shown at the mid-brain hind-brain boundary (MHB) (Hirate &
335 Okamoto, 2006). Subsequent studies in mouse also reported *Cnpy1* mRNA at the MHB
336 (Paek *et al*, 2012). In contrast, we found *Cnpy1* mRNA in the VNO and MOE, but Cnpy1
337 protein only in the VNO. We propose that mouse *Cnpy1* is post-transcriptionally regulated,
338 without a role for Cnpy1 protein in the MOE or MHB. The absence of developmental defects
339 in our *Cnpy1* gene deletion mouse model supports this hypothesis. While the existence of
340 an as-yet undescribed alternate transcript cannot be ruled out, our Cnpy1 knockout allele
341 and anti-Cnpy1 antibody binding motif are likely to be common to all potential isoforms,
342 arguing against such a possibility.
343
344 Our experiments reveal that Cnpy1 plays an essential, non-redundant role in Gαo VSNs.
345 Intracellular localization of Cnpy1 in VNO sections as well as expression of the cloned gene
346 in heterologous cells demonstrates an ER localization. IP-proteomics from the VNO,
347 identified Cnpy1 interactions with multiple V2R GPCRs as well as specific ER chaperones
348 such as Hsp90b1, Dnajc3, Calnexin, Calr4. Mammalian Cnpy homologs, Cnpy2 - Cnpy5 are
349 known to function as ER co-chaperones. Cnpy3, Cnpy4 (also termed PRAT4A, 4B), along
350 with Hsp90 family proteins co-chaperone the folding and exit of Toll-like receptors in the ER
351 of immune cells (Hart & Tapping, 2012; Hong *et al*, 2017b; Konno *et al.*, 2006; Shibata *et al.*,
352 2012; Takahashi *et al*, 2007; Wakabayashi *et al.*, 2006). Likewise, Cnpy5 (also termed
353 ERp1/MZB1), interacting with Grp94 and BiP, is an essential ER chaperone for the folding
354 and secretion of immunoglobulins in B cells (Rosenbaum *et al*, 2014; Shimizu *et al.*, 2009;
355 van Anken *et al.*, 2009; Xiong *et al*, 2019). These studies along with our results, would point
356 to a mechanistic role for mouse Cnpy1 in co-chaperoning V2R GPCRs.
357
358 On the contrary, Cnpy1 deletion did not impair ER export and dendritic targeting of V2Rs in
359 our mouse model. Instead, Cnpy1$^{-/-}$ Gαo neurons exhibited reduced responses to VNO
360 stimuli. While mice lacking Cnpy1 were born with normal number of VSNs, Gαo neurons
361 were progressively and selectively lost during postnatal development due to apoptosis. A
362 similar pattern of gradual postnatal loss of Gαo VSNs has been described in mice lacking
363 the Gαo G-protein subunit, essential for V2R signal transduction (Chamero *et al.*, 2011;

364 Tanaka *et al*, 1999). Neurons in mice engineered to render a V2R non-functional, by insertion
365 of LacZ in the coding region (Belluscio *et al.*, 1999), also showed a gradual postnatal loss.
366 Similar results have been described in mouse models lacking a functional V1R (Rodriguez
367 *et al.*, 1999) or the cognate Gαi2 subunit (Norlin *et al*, 2003). Likewise, mice lacking TRPC2,
368 the major vomeronasal ion-channel thought to be downstream of GPCR signaling, also show
369 postnatal VSN degeneration (Stowers *et al*, 2002). Collectively these studies highlight that
370 functional vomeronasal GPCR signaling is essential for postnatal neuronal survival. We
371 therefore propose that Cnpy1 is required in the ER of Gαo VSNs to assemble signaling-
372 competent V2R GPCRs, the absence of which triggers apoptosis. V2Rs belong to the class-
373 C GPCR family, that contain a large extracellular ligand binding Venus fly-trap domain, in
374 addition to 7-transmembrane domains. Similar to other class-C GPCRs, V2Rs are also likely
375 to function as obligate homo or heterodimers. The assembly and export of functional V2Rs
376 may require participation of multiple ER chaperones, some of which could be Gαo VSN
377 subtype specific. For instance, Cnpy1 could affect the local folding, conformational states,
378 post translational modifications of V2Rs or their dimerization, interactions with G-proteins –
379 any of which could disrupt signaling, while escaping ER quality control.
380
381 While we observed substantial loss of V2R expressing neurons in p60 Cnpy1 null mice,
382 some neurons persisted. Gαo neurons may differ in their individual susceptibility to a loss of
383 receptor signaling, depending on the V2R they express. In the main olfactory system,
384 receptor identity has been shown to determine ER stress levels across neurons (Shayya *et*
385 *al*, 2022). The mechanisms of sensory GPCR induced ER stress may operate differently in
386 the VNO (Dalton *et al*, 2018), although it is conceivable that Cnpy1 via its interaction with
387 V2Rs, could also impact ER stress levels. For instance, Cnpy2 has been shown function in
388 context specific manner during ER stress either by activating the UPR or by reducing stress
389 (Hong *et al.*, 2017a; Scordino *et al*, 2024). An alternate possibility could be that some of the
390 Cnpy1$^{-/-}$ VSNs that do not form a signaling competent V2R, may switch to transcribe another
391 V2R, which may transiently prolong their apoptosis.
392
393 In summary, our findings establish mouse Cnpy1 as a novel VNO specific ER chaperone,
394 required for the survival of Gαo neurons. In conjunction with other ER
395 chaperones, *Cnpy1* likely contributes to the assembly of signaling-competent V2R GPCR

396 complexes, opening new avenues for dissecting molecular mechanisms of vomeronasal
397 receptor function.

398 **Materials and Methods**

399

400 Animals:

401 All experiments were carried out with approval from the Institutional Animal Ethics
402 Committee (Protocol numbers TIFRH/2019/02, TIFRH/2021/10). C57BL/6J
403 (RRID:IMSR_JAX:000664) and V2r1b-IRES-tauGFP (RRID:IMSR_JAX:006657) mice, were
404 purchased from JAX, housed and bred in individually ventilated cages, in a specific
405 pathogen-free barrier facility, with a 12-hour light-dark cycle, ad-libitum provision of feed and
406 water. Tunicamycin treatment was performed by intraperitoneal injection of 9-week-old
407 C57BL/6J mice at a dose of 2 mg/kg body weight. Liver tissue was collected 48 hours after
408 injection.

409

410 Cnpy-1 gene deletion mice were generated using CRISPR-Cas9 in the following manner.
411 CRISPR gRNA sequence: $^{5'}$GATATTCGAACTTATTGCCC$^{3'}$ was cloned into BbsI digested
412 pX330 plasmid (Addgene# 42230). In-vitro gRNA activity was assessed by transfecting N2A
413 cells with the cloned g-RNA, followed by T7E1 assay using standard methods (Ran *et al*,
414 2013). T7 sgRNA and Cas9 template was PCR amplified, gel purified, and in vitro
415 transcribed, after which the purified RNA was microinjected into B6/CBA zygotes at a
416 concentration of 50ng/ul Cas9 and 25ng/ul gRNA. One-cell fertilized embryos were injected
417 into the pronucleus and cytoplasm of each zygote. Microinjections and mouse transgenesis
418 experiments were performed as described previously (Behringer, 2014; Pease *et al*, 2011).
419 Global knockout alleles were detected by PCR across the cleavage site, followed by T7E1
420 assay. Oligo sequences and band sizes: ~280bp band cleaves to ~180bp and ~100bp.
421 Forward primer: 5' GGA GCC CTG TCC ATG TGT CTC TGC TCA CAC 3'
422 Reverse primer: 5' TCT GGT CCC CAG AAG TCT GTG TAG AGC CAG 3'
423 Animals identified to contain the gene deletion allele by T7E1 assay were bred with
424 C57BL/6J and offspring were analyzed by PCR, T7E1 and confirmed by Sanger sequencing.
425 One of the lines resulting in a 99 base pair deletion (Chromosome 5: 28412242-28412340
426 as per mouse genome reference GRCm39) was confirmed for lack of Cnpy1 protein by anti-
427 Cnpy1 labeling on VNO sections, western blot from VNO lysates. Mice containing this gene
428 deletion allele were backcrossed for 8 generations to C57Bl/6J to generate a 98% pure
429 background.

430

431 Antibody generation:

432 Anti-peptide antibodies were generated by identifying amino acid sequence specific to the
433 target protein and based on its predicted immunogenicity. KLH conjugated synthetic
434 peptides were injected into rabbits to generate polyclonal antibodies, by YenZym Antibodies
435 (Brisbane, CA). Antibodies were peptide affinity purified and dialyzed against PBS. Antibody
436 specificity was confirmed via detection of target protein on tissue sections, as well as by
437 blocking reactivity by pre-incubation with the peptide used for immunization (**Figure S7**).
438 The following mouse peptide sequences from target proteins were used:

439 1. Cnpy1: DDPVTKQKYFRRYAPRKGD
440 2. Vmn2r111/Vmn2r112: FWKMKRNENKDRNQ
441 3. Vmn2r65: QKVNFTQKFSDTHSKIEYNH

442

443 Tissue Panel RT-PCR:

444 RNA was isolated from various tissues harvested from 12-week old C57BL/6J mice using
445 the TRIzol reagent (Invitrogen #15596026) as per the manufacturer guidelines. cDNA was
446 synthesized with 0.6ug of RNA from tissue using Superscript IV c-DNA synthesis kit (Thermo
447 Fisher Scientific) with oligodT as per manufacturer instructions. cDNA was purified using a
448 DNA cleanup kit (Monarch, NEB) and used as a template for performing PCR with primers
449 targeting exon-1 or exon-2 of full-length *Cnpy1* and *Gapdh* as positive control.

450 Exon1-2 _FP TTTGGAGAGACATGGGGCTCG
451 Exon1-2_RP GGAGCCCACCTTGGTTTTC
452 Exon2-3_FP CCCTGATGGACGAGGTGGAGTA
453 Exon2-3_RP CGATGAGGAACGCCTCGGAC

454

455 RNA sequencing and analysis:

456 The full-length Cnpy1 transcript sequence was obtained using VNO RNA-seq FASTQ files
457 from Santoro et al. to assemble the transcriptome. Raw reads were aligned to the mm10
458 reference genome using STAR, and the resulting BAM files were used as input for
459 transcriptome assembly with StringTie.

460

461 VNO from Cnpy1$^{+/+}$ and Cnpy1$^{-/-}$ littermate animals (three each) were dissected. Lysis was
462 performed in a Beadruptor using RLT buffer of Qiagen Rneasy plus kit with 1.4mm ceramic
463 beads, and RNA was isolated as per manufacturer instructions. RNA was quantified using
464 Qubit RNA BR assay kit and quality was checked using RNA Screen Tapes (Agilent,
465 Cat#5067-5576)/RNA HS ScreenTapes (Agilent, Cat#5067-5579). 500ng RNA from each
466 sample was used for library preparation using NEB Ultra II directional RNA-seq library prep
467 kit (NEB #E7765S). Initially, poly-A containing mRNA were purified using oligo-dT magnetic
468 beads from NEBNext Poly(A) magnetic isolation module (NEB #E7490). Following
469 purification, the library was prepared as per manufacturer's instructions. The libraries were
470 indexed using NEBNext Multiplex Oligos for Illumina 96 Unique Dual Index Primer 96 rxn
471 Set 3. Prepared libraries were quantified using Qubit HS Assay and pooled. Pooled libraries
472 were sequenced on Illumina Novaseq instrument at 150bp paired end configuration to obtain
473 20Gb data per sample. Adaptor contamination was removed from the samples using
474 trim_galore tool and Salmon tool was used to quantify the gene expression. Raw counts
475 from Salmon were used as input for DeSeq2 to perform differential expression analysis
476 between Cnpy1$^{-/-}$ and Cnpy1$^{+/+}$. pHeatmap R package was used to generate the heatmap
477 of differentially expressed genes with an adjusted p-value < 0.01 and absolute foldchange
478 of 1.5.
479
480 qPCR validation of RNAseq results:
481 RNA isolation was done as described above. cDNA was prepared with 1ug of RNA using
482 Superscript IV cDNA synthesis kit and the same was used for qPCR reactions as a template.
483 TaqMan probes specific to each gene were used to set up 10uL reaction for each probe in
484 triplicates using Cnpy1$^{-/-}$ and Cnpy1$^{+/+}$ cDNA samples as templates as per the TaqMan
485 master mix manual. qPCR was performed on Roche lightCycler96 instrument, and data was
486 exported, analyzed using the supplied software. Expression of each gene was normalized
487 by Gapdh expression in that sample and represented as relative to Cnpy1$^{+/+}$.
488
489 RNA *in situ* hybridization (ISH):
490 Chromogenic RNA ISH was performed as described before (Devakinandan *et al.*, 2024).
491 Briefly, using VNO cDNA as template and primers containing T7 RNA polymerase promoter
492 sequence, specific region of Cnpy1 coding sequence was PCR amplified. *In-vitro*

493 transcription was performed using Digoxigenin (DIG) labeled UTP nucleotide mix and post
494 RNA cleanup, riboprobes were stored at -80°C. Freshly dissected VNO was embedded in
495 OCT and cryosectioned at 14µm thickness. Tissue sections captured on superfrost-plus
496 slides were hybridized with Cnpy1 specific riboprobe, washed and hybridized probe was
497 detected using anti-DIG conjugated with alkaline phosphatase. Colorimetric (BCIP/NBT)
498 substrates were used to develop the bound antibody-enzyme conjugate reactions.
499 Cnpy1_ISH_F CCGAGGCGTTCCTCATCGAC
500 Cnpy1_ISH_R TAATACGACTCACTATAGGGTGACTGAGAGGGGTGGCTTT
501
502 Cnpy1 expression in heterologous cells:
503 Mouse Cnpy1 corresponding to the full-length sequence (Figure1) was cloned by PCR
504 amplification from VNO cDNA into pcDNA3.1+ or pcDNA4TO plasmids. Myc tag was added
505 after the start codon or before the stop codon, to generate myc-Cnpy1 and Cnpy1-myc
506 clones in the same plasmid vector. HEK293 cells, cultured under 5% CO_2 in Dulbeco's
507 Modified Eagle Medium (DMEM) supplemented with GlutaMAX (Gibco), penicillin-
508 streptomycin (Sigma) and 5% FBS, were adhered to poly-D lysine coated 35mm glass
509 coverslip bottom dishes. Plasmid DNA was transfected using Polyethylenimine (PEI, Sigma)
510 transfection reagent. 18-24 hours post transfection; cells were fixed with 2%
511 paraformaldehyde and expressed protein was detected using immunofluorescence
512 microscopy.
513
514 Immunofluorescence microscopy:
515 VNO tissues, either with or without outer bone, were harvested from animals, fixed for 10-
516 20 minutes with 4% Paraformaldehyde (PFA, Electron Microscopy Sciences) in phosphate
517 buffered saline (PBS). After washing off PFA, tissues with bone were treated with 0.5M EDTA
518 for 2-16 hours (depending on mouse age) to soften the bone, followed by cryoprotection with
519 30% sucrose and embedding, freezing in OCT (Sakura) medium. 14µm sections were
520 collected on superfrost-plus slides using a cryostat and fixed with 4% PFA. Unreacted PFA
521 was quenched with 30mM glycine in PBS for 10 minutes. Sections were blocked and
522 permeabilized using 3% bovine serum albumin (BSA) in 0.1% Triton-X 100 (0.1% Nonidet
523 P40 for HEK293) detergent and labeled with primary antibodies diluted in the same blocking
524 buffer. The respective primary antibodies were detected using Alexa Fluor 488, Cy3 or Alexa

525 Fluor 647 fluorophore conjugated secondary antibodies (Jackson ImmunoResearch).
526 Images were acquired on Olympus FV3000, Leica Stellaris confocal microscopes using
527 10X-0.2NA air or 60X-1.4NA oil immersion objectives with sequential channel image
528 acquisition. Images for quantification of Gαi2, Gαo zones, CC3, V2Rs or Ki67 fluorescence
529 were acquired on Olympus IX83 inverted fluorescence microscope operating in widefield
530 mode.
531
532 Image quantification:
533 Fluorescent labeled cells from images of VNO sections (anti-CC3, anti-Ki67, anti-Vmn2r,
534 anti-SEKDEL) were quantified automatically using ilastik tool (Berg *et al*, 2019). To avoid
535 estimation errors caused by fluorescence from non-sensory epithelium, sensory epithelium
536 was manually cropped in each section. Pixel classification in ilastik was trained on 10-15
537 representative images, using features including intensity and edge detection to differentiate
538 truly labeled pixels from background. Next, object identification in ilastik was trained with
539 pixel classification data to identify VSN cell bodies and exclude objects below a minimum
540 size threshold. The program was also trained to classify single cells, doublets, or multiplets.
541 Once identification was optimized separately for each antibody, batch processing was
542 performed to produce data tables for each image. These tables were parsed with custom
543 Python code, which summed singlets, doublets, and multiplets per image to calculate total
544 cell counts. To quantify CC3 and SEKDEL double-positive cells, segmented masks of the
545 SEKDEL-labeled area were generated using pixel classification workflow, applied to the CC3
546 channel, and the above quantification workflow was used for CC3+ cells. The area of
547 SEKDEL labeling was measured from the segmented mask. Representative images for the
548 steps in this process are shown in **Figure S8**. Quantification of Gαo, Gαi2 (anti-Nsg1) area
549 in Figure 4 and pS6+ cells in Figure 8 was done manually.
550
551 Western Blot:
552 VNOs pooled from 2-5 mice were lysed by passing through 10-20 strokes of a Dounce
553 homogenizer using lysis (50mM Tris - pH7.5, 150mM NaCl, 1mM EDTA, 1% Nonidet-P40,
554 1mM PMSF, Protease inhibitor cocktail) on ice. To ensure complete homogenization, tissues
555 were disrupted in Beadruptor, using 2.8mm and 1.4mm ceramic beads. Lysate was clarified
556 by removing debris by centrifugation at 20000xg at 4°C and used for total protein estimation

557 via the BCA method (Thermo). Tissue or cell lysate was mixed with Laemmli sample buffer,
558 containing fresh DTT and heated at 90°C for 3 minutes before loading on a discontinuous
559 12% SDS-polyacrylamide gel. To detect Cnpy1, gel was stopped just before the dye front
560 ran out and transferred to 0.2 µm PVDF membrane, followed by blocking membrane with
561 5% non-fat milk powder in 1X PBA and Tween-20 and application of Cnpy1 primary antibody,
562 Donkey anti-Rabbit HRP conjugate secondary antibody (Jackson ImmunoResearch).
563 Chemiluminescence was detected using ECL Plus kit (Cytiva) on a chemidoc (Vilbur
564 instruments).
565
566 VNO lysate and immunoprecipitation (IP):
567 $IP_{Cnpy1:B6}$ and $IP_{Cnpy1:KO}$, were performed as three technical replaces, and $IP_{IgG:B6}$ as 2
568 replicates. Each replicate comprised of VNOs collected from 50 mice of 8-16 weeks age and
569 roughly equal numbers of male and female. VNOs were dissected, pooled and kept frozen
570 at -80°C. On the day of experiment, tubes containing VNOs were thawed and transferred to
571 a 2ml Dounce homogenizer with cold lysis buffer. Homogenization was performed as
572 described above. Cell debris was pelleted by centrifugation at 15000 rpm at 4°C for 15 min
573 and supernatant was transferred to a new tube. After 2 hours of preclearing with Protein-A
574 Mag Sepharose beads (Cytiva), 15µg of Cnpy1 antibody or normal rabbit IgG (Jackson
575 ImmunoResearch) was added to each tube. After 16 hours of antibody incubation on end-
576 to-end rotator at 4°C, antibodies were precipitated by adding mag-sepharose beads for 4
577 hours. Magnetic beads containing antibody-protein complex were retained using magnetic
578 racks, washed three times with lysis buffer. Elution of antibodies from Protein-A beads was
579 performed with 2X Laemmli buffer at 95°C. The eluate was used for mass spectrometry.
580
581 Sample preparation for quantitative mass spectrometry (MS):
582 The SP3 protocol (Hughes *et al*, 2014; Hughes *et al*, 2019) was performed on a KingFisher
583 system (Thermo) for sample clean-up. Trypsin (sequencing grade, Promega) was added in
584 an enzyme to protein ratio 1:20 for a 5h digestion at 37°C (in 50 mM HEPES) together with
585 5mM tris(2-carboxyethyl)phosphine and 20mM 2-chloroacetamide.
586 Peptides were labelled with TMT10plex isobaric labeling reagent (Thermo) (Werner *et al*,
587 2014) according to the manufacturer's instructions. In brief, of 0.8mg reagent dissolved in
588 42ul acetonitrile (100%) 8 ul was added and incubated for 1h room temperature. The

589 reaction was stopped with 8 ul 5% hydroxylamine for 15 minutes at RT. Samples of a set
590 were combined and desalted on a OASIS® HLB µElution Plate (Waters). Offline high pH
591 reverse phase fractionation was carried out on an Agilent 1200 Infinity high-performance
592 liquid chromatography system, equipped with a Gemini C18 column (3 µm, 110 Å, 100 x 1.0
593 mm, Phenomenex) installed with a Gemini C18, 4 x 2.0 mm SecurityGuard (Phenomenex)
594 cartridge as a guard column. The binary solvent system consisted of 20 mM ammonium
595 formate (pH 10.0) (A) and 100% acetonitrile as mobile phase (B). The flow rate was set to
596 0.1 mL/min. Peptides were separated using a gradient of 100% A for 2 min, to 35% B in 59
597 min, to 85% B in another 1 min and kept at 85% B for an additional 15 min, before returning
598 to 100% A and re-equilibration for 13 min. 48 fractions were collected which were pooled
599 into 6 fractions. Pooled fractions were dried under vacuum centrifugation, reconstituted in
600 10 µL 1% formic acid, 4% acetonitrile and then stored at -80 °C until LC-MS analysis.
601
602 MS data acquisition:
603 An UltiMate 3000 RSLC nano LC system (Dionex) fitted with a trapping cartridge (µ-
604 Precolumn C18 PepMap 100, 5µm, 300 µm i.d. x 5 mm, 100 Å) and an analytical column
605 (nanoEase™ M/Z HSS T3 column 75 µm x 250 mm C18, 1.8 µm, 100 Å, Waters) was
606 coupled to an Q-Exactive Plus Mass Spectrometer (Thermo) using the Nanospray Flex™
607 ion source in positive ion mode.
608 The samples were loaded onto the trapping column with a constant flow of 30 µL/min 0.05%
609 trifluoroacetic acid in water for 4 minutes. After switching in line with the analytical column
610 peptides were eluted at a constant flow of 0.3 µL/min using the method described in the
611 following. The binary solvent system consisted of 0.1% formic acid in water with 3% DMSO
612 (solvent A) and 0.1% formic acid in acetonitrile with 3% DMSO (solvent B). The percentage
613 of solvent B was increased from 2% to 8% in 2 min, from 8% to 28% in 66 min, from 28%-
614 40% in another 10 min and finally from 40%-80% in 2.5 min, followed by re-equilibration
615 back to 2% B in 5.5 min.
616 The peptides were introduced into the MS instrument via a Pico-Tip Emitter 360 µm OD x
617 20 µm ID; 10 µm tip (CoAnn Technologies) and an applied spray voltage of 2.4 kV. The
618 capillary temperature was set at 275°C. Full mass scan was acquired with a mass range
619 375-1200 m/z in profile mode in the orbitrap with resolution of 70000. The fill time was set
620 at a maximum of 250 ms with a limitation of $3x10^6$ ions. Data dependent acquisition (DDA)

621 was performed with the resolution of the Orbitrap set to 35000, with a fill time of 120 ms and
622 a limitation of $2x10^5$ ions. A normalized collision energy of 32 was applied. MS^2 data was
623 acquired in profile mode. Define first mass was set to 110 m/z.
624
625 MS - data analysis:
626 Fragpipe v21.1 with MS Fragger v4.0 was used to process the acquired data, which was
627 searched against a mus musculus proteome database (UP000000589, 21968entries,
628 October 2022) plus common contaminants and reversed sequences. The following
629 modifications were included into the search parameters: Carbamidomethyl on Cysteine and
630 TMT10 on lysine as fixed modifications, protein N-term acetylation, oxidation on methionine
631 and TMT10 on N-termini as variable modifications. A mass error tolerance of 20 ppm was
632 used for precursor as well as for fragment ions. Trypsin was set as protease with a maximum
633 of two missed cleavages. The minimum peptide length was set to seven amino acids. The
634 false discovery rate on peptide and protein level was set to 0.01.
635
636 The raw output files of FragPipe (protein.tsv files) were processed using the R programming
637 language. Contaminants and reverse proteins were filtered out and only proteins that were
638 quantified with at least 2 razor peptides (Razor.Peptides >= 2) were considered for the
639 analysis. 1980 proteins passed the quality control filters. Log2 transformed raw TMT reporter
640 ion intensities ('channel' columns) were first cleaned for batch effects using the
641 'removeBatchEffect' function of the limma package and further normalized using the
642 'normalizeVSN' function of the limma package. Proteins were tested for differential
643 expression using a moderated t-test by applying the limma package ('lmFit' and 'eBayes'
644 functions). The replicate information was added as a factor in the design matrix given as an
645 argument to the 'lmFit' function of limma. A protein was annotated as an enriched hit with a
646 false discovery rate (fdr) smaller than 0.05 and absolute fold change >= 2; or as a hit with a
647 fdr below 0.05 and an absolute fold change between 1.5 and 2.0 in each comparison. The
648 common enriched hits between $IP_{Cnpy1:B6}$ vs $IP_{IgG:B6}$ and $IP_{Cnpy1:B6}$ vs $IP_{Cnpy1:KO}$ were
649 considered as potential interacting proteins of Cnpy1.
650
651 Rat and opposite sex bedding exposure:

652 Male Cnpy1$^{+/+}$ and Cnpy1$^{-/-}$ mice aged 10–11 weeks were individually housed and isolated
653 for a minimum of three days. Following isolation, soiled bedding collected from three male
654 Wistar rats housed together was introduced into the home cage of each mouse. After one
655 hour of exposure to rat bedding, the mice were euthanized, and VNOs were dissected.
656 Female or male bedding was freshly collected from group housed adult females and the
657 same procedure was followed. The VNO tissues were fixed in 4% paraformaldehyde for four
658 hours and subsequently cryoprotected with 30% sucrose overnight. Immunohistochemistry
659 for pS6 and SEKDEL was performed according to the procedure described above. Cells
660 positive for pS6 within SEKDEL-labeled regions or throughout the neuroepithelium were
661 counted manually.
662
663 Resident-intruder assay:
664 Castration of C57Bl/6J mice was performed by orchidectomy procedure, performed on 6–8
665 weeks old C57BL/6J males chosen to be 10% lighter in weight than residents. Mice were
666 anesthetized with Ketamine-Xylazine, followed by Meloxicam and Ceftriaxone-Tazobactam.
667 After making a midline incision in the scrotum, both testes were exteriorized, ligated and
668 removed. The incision was closed with sutures, iodine and antiseptic powder were applied,
669 and mice were allowed 10 days for recovery.
670
671 Cnpy1$^{+/+}$, Cnpy1$^{+/-}$ and Cnpy1$^{-/-}$ male mice from Cnpy1$^{+/-}$ x Cnpy1$^{+/-}$ of 10-12 weeks age were
672 individually co-housed with a female for five days, followed by removal of the females.
673 Starting one hour after the onset of the dark phase, castrated C57BL/6J males (intruder),
674 swabbed with fresh urine from intact C57BL/6J males, were introduced into the home cage
675 of the resident male for 10 minutes daily over four consecutive days, comprising the training
676 phase. On the fifth day, resident-intruder interactions were recorded under infrared
677 illumination using two Hikvision CCTV cameras from the top and side of the resident's home
678 cage. Aggressive behaviors, including attacks, chases, and wrestling, were manually scored
679 from within the first 10 minutes of the video recordings. Resident and intruder males were
680 separated after 15 minutes, or earlier, in case of extremely aggressive interactions. Scoring
681 and quantification of aggressive behaviors was done by blinding the genotype. Two Cnpy1$^{+/+}$
682 males that did not show any aggressive behavior during the training phase were excluded.
683

Acknowledgements

We acknowledge part support from the Hope Center viral vectors and Mouse Genetics Core facilities at Washington University School of Medine, St. Louis, MO in generation of Cnpy1 gene deletion mouse model; We thank Jennifer Schwarz and Frank Stein of the Proteomics Core Facility at EMBL Heidelberg for help with peptide mass-spectrometry and analysis; Roberto Tirindelli for gift of the anti-pan family-D V2R antibody; Sritama Datta for technical assistance, Gopalkrishna R. for training with mouse surgery; Ganesh Kadasoor for assistance with CellSens imaging software. This work funded by Department of Atomic Energy, Government of India (Project No RTI 4007) and NIH Grant R21 MH099798.

Data Availability

Mouse Cnpy1 transcript sequence is submitted to GenBank accession ID: PX423936. IP-mass spectrometry proteomics data was deposited to the ProteomeXchange Consortium via PRIDE partner repository with dataset identifier PXD068826.

References

Baker EK, Colley NJ, Zuker CS (1994) The cyclophilin homolog NinaA functions as a chaperone, forming a stable complex in vivo with its protein target rhodopsin. *EMBO J* 13: 4886–4895

Behringer R (2014) *Manipulating the mouse embryo : a laboratory manual*. Cold Spring Harbor Laboratory Press, Cold Spring Harbor, New York

Belluscio L, Koentges G, Axel R, Dulac C (1999) A map of pheromone receptor activation in the mammalian brain. *Cell* 97: 209–220

Berg S, Kutra D, Kroeger T, Straehle CN, Kausler BX, Haubold C, Schiegg M, Ales J, Beier T, Rudy M *et al* (2019) ilastik: interactive machine learning for (bio)image analysis. *Nat Methods* 16: 1226–1232

Brann JH, Firestein S (2010) Regeneration of new neurons is preserved in aged vomeronasal epithelia. *J Neurosci* 30: 15686–15694

Chamero P, Katsoulidou V, Hendrix P, Bufe B, Roberts R, Matsunami H, Abramowitz J, Birnbaumer L, Zufall F, Leinders-Zufall T (2011) G protein G(alpha)o is essential for vomeronasal function and aggressive behavior in mice. *Proc Natl Acad Sci U S A* 108: 12898–12903

Chamero P, Marton TF, Logan DW, Flanagan K, Cruz JR, Saghatelian A, Cravatt BF, Stowers L (2007) Identification of protein pheromones that promote aggressive behaviour. *Nature* 450: 899–902

Dalton RP, Karagöz GE, Kahiapo J, Sharma R, Bashkirova LE, Lyons DB, Matsunami H, Walter P (2018) Olfactory and Vomeronasal Receptor Feedback Employ Divergent Mechanisms of PERK Activation. *bioRxiv*: 239830

Del Punta K, Puche A, Adams NC, Rodriguez I, Mombaerts P (2002) A divergent pattern of sensory axonal projections is rendered convergent by second-order neurons in the accessory olfactory bulb. *Neuron* 35: 1057–1066

Devakinandan GVS, Terasaki M, Dani A (2024) Single-cell transcriptomics of vomeronasal neuroepithelium reveals a differential endoplasmic reticulum environment amongst neuronal subtypes. *Elife* 13

Dey S, Matsunami H (2011) Calreticulin chaperones regulate functional expression of vomeronasal type 2 pheromone receptors. *Proc Natl Acad Sci U S A* 108: 16651–16656

Dwyer ND, Troemel ER, Sengupta P, Bargmann CI (1998) Odorant receptor localization to olfactory cilia is mediated by ODR-4, a novel membrane-associated protein. *Cell* 93: 455–466

Hart BE, Tapping RI (2012) Cell surface trafficking of TLR1 is differentially regulated by the chaperones PRAT4A and PRAT4B. *J Biol Chem* 287: 16550–16562

Hirate Y, Okamoto H (2006) Canopy1, a novel regulator of FGF signaling around the midbrain-hindbrain boundary in zebrafish. *Curr Biol* 16: 421–427

Hong F, Liu B, Wu BX, Morreall J, Roth B, Davies C, Sun S, Diehl JA, Li Z (2017a) CNPY2 is a key initiator of the PERK-CHOP pathway of the unfolded protein response. *Nat Struct Mol Biol* 24: 834–839

Hong F, Mohammad Rachidi S, Lundgren D, Han D, Huang X, Zhao H, Kimura Y, Hirano H, Ohara O, Udono H *et al* (2017b) Mapping the Interactome of a Major Mammalian Endoplasmic Reticulum Heat Shock Protein 90. *PLoS One* 12: e0169260

Hughes CS, Foehr S, Garfield DA, Furlong EE, Steinmetz LM, Krijgsveld J (2014) Ultrasensitive proteome analysis using paramagnetic bead technology. *Mol Syst Biol* 10: 757

Hughes CS, Moggridge S, Muller T, Sorensen PH, Morin GB, Krijgsveld J (2019) Single-pot, solid-phase-enhanced sample preparation for proteomics experiments. *Nat Protoc* 14: 68–85

Ishii T, Mombaerts P (2011) Coordinated coexpression of two vomeronasal receptor V2R genes per neuron in the mouse. *Mol Cell Neurosci* 46: 397–408

Isogai Y, Si S, Pont-Lezica L, Tan T, Kapoor V, Murthy VN, Dulac C (2011) Molecular organization of vomeronasal chemoreception. *Nature* 478: 241–245

Katreddi RR, Taroc EZM, Hicks SM, Lin JM, Liu S, Xiang M, Forni PE (2022) Notch signaling determines cell-fate specification of the two main types of vomeronasal neurons of rodents. *Development* 149

751 Kimoto H, Haga S, Sato K, Touhara K (2005) Sex-specific peptides from exocrine glands
752 stimulate mouse vomeronasal sensory neurons. *Nature* 437: 898–901

753 Konno K, Wakabayashi Y, Akashi-Takamura S, Ishii T, Kobayashi M, Takahashi K, Kusumoto Y,
754 Saitoh S, Yoshizawa Y, Miyake K (2006) A molecule that is associated with Toll-like receptor 4
755 and regulates its cell surface expression. *Biochem Biophys Res Commun* 339: 1076–1082

756 Lee D, Kume M, Holy TE (2019) Sensory coding mechanisms revealed by optical tagging of
757 physiologically defined neuronal types. *Science* 366: 1384–1389

758 Liberles SD (2014) Mammalian pheromones. *Annu Rev Physiol* 76: 151–175

759 Loconto J, Papes F, Chang E, Stowers L, Jones EP, Takada T, Kumanovics A, Fischer Lindahl K,
760 Dulac C (2003) Functional expression of murine V2R pheromone receptors involves selective
761 association with the M10 and M1 families of MHC class Ib molecules. *Cell* 112: 607–618

762 Nakano H, Iida Y, Suzuki M, Aoki M, Umemura M, Takahashi S, Takahashi Y (2016) Activating
763 transcription factor 5 (ATF5) is essential for the maturation and survival of mouse basal
764 vomeronasal sensory neurons. *Cell Tissue Res* 363: 621–633

765 Norlin EM, Gussing F, Berghard A (2003) Vomeronasal phenotype and behavioral alterations in
766 G alpha i2 mutant mice. *Curr Biol* 13: 1214–1219

767 Ohta Y, Ichimura K (2000) Proliferation markers, proliferating cell nuclear antigen, Ki67, 5-
768 bromo-2'-deoxyuridine, and cyclin D1 in mouse olfactory epithelium. *Ann Otol Rhinol Laryngol*
769 109: 1046–1048

770 Paek H, Antoine MW, Diaz F, Hebert JM (2012) Increased beta-catenin activity in the anterior
771 neural plate induces ectopic mid-hindbrain characteristics. *Dev Dyn* 241: 242–246

772 Pease S, Saunders TL, International Society for Transgenic Technologies. (2011) *Advanced*
773 *protocols for animal transgenesis : an ISTT manual*. Springer, Heidelberg ; New York ;

774 Ran FA, Hsu PD, Wright J, Agarwala V, Scott DA, Zhang F (2013) Genome engineering using the
775 CRISPR-Cas9 system. *Nat Protoc* 8: 2281–2308

776 Rodriguez I, Feinstein P, Mombaerts P (1999) Variable patterns of axonal projections of sensory
777 neurons in the mouse vomeronasal system. *Cell* 97: 199–208

778 Rosenbaum EE, Brehm KS, Vasiljevic E, Liu CH, Hardie RC, Colley NJ (2011) XPORT-dependent
779 transport of TRP and rhodopsin. *Neuron* 72: 602–615

780 Rosenbaum EE, Hardie RC, Colley NJ (2006) Calnexin is essential for rhodopsin maturation,
781 Ca2+ regulation, and photoreceptor cell survival. *Neuron* 49: 229–241

782 Rosenbaum M, Andreani V, Kapoor T, Herp S, Flach H, Duchniewicz M, Grosschedl R (2014)
783 MZB1 is a GRP94 cochaperone that enables proper immunoglobulin heavy chain biosynthesis
784 upon ER stress. *Genes Dev* 28: 1165–1178

785 Saito H, Kubota M, Roberts RW, Chi Q, Matsunami H (2004) RTP family members induce
786 functional expression of mammalian odorant receptors. *Cell* 119: 679–691

787 Salazar I, Sanchez Quinteiro P (2003) Differential development of binding sites for four lectins
788 in the vomeronasal system of juvenile mouse: from the sensory transduction site to the first
789 relay stage. *Brain Res* 979: 15–26

790 Santoro SW, Jakob S (2018) Gene expression profiling of the olfactory tissues of sex-separated
791 and sex-combined female and male mice. *Sci Data* 5: 180260

792 Schildknegt D, Lodder N, Pandey A, Chatsisvili A, Egmond M, Pena F, Braakman I, van der Sluijs
793 P (2019) Characterization of CNPY5 and its family members. *Protein Sci* 28: 1276–1289

794 Scordino M, Stepanova P, Srinivasan V, Pham DD, Eriksson O, Lalowski M, Mudo G, Di Liberto V,
795 Korhonen L, Voutilainen MH *et al* (2024) CNPY2 protects against ER stress and is expressed by
796 corticostriatal neurons together with CTIP2 in a mouse model of Huntington's disease. *Front*
797 *Mol Neurosci* 17: 1473058

798 Sharma R, Ishimaru Y, Davison I, Ikegami K, Chien MS, You H, Chi Q, Kubota M, Yohda M, Ehlers
799 M *et al* (2017) Olfactory receptor accessory proteins play crucial roles in receptor function and
800 gene choice. *Elife* 6

801 Shayya HJ, Kahiapo JK, Duffie R, Lehmann KS, Bashkirova L, Monahan K, Dalton RP, Gao J, Jiao
802 S, Schieren I *et al* (2022) ER stress transforms random olfactory receptor choice into axon
803 targeting precision. *Cell* 185: 3896–3912 e3822

804 Shibata T, Takemura N, Motoi Y, Goto Y, Karuppuchamy T, Izawa K, Li X, Akashi-Takamura S,
805 Tanimura N, Kunisawa J *et al* (2012) PRAT4A-dependent expression of cell surface TLR5 on
806 neutrophils, classical monocytes and dendritic cells. *Int Immunol* 24: 613–623

807 Shimizu Y, Meunier L, Hendershot LM (2009) pERp1 is significantly up-regulated during plasma
808 cell differentiation and contributes to the oxidative folding of immunoglobulin. *Proc Natl Acad*
809 *Sci U S A* 106: 17013–17018

810 Silvotti L, Cavalca E, Gatti R, Percudani R, Tirindelli R (2011) A recent class of chemosensory
811 neurons developed in mouse and rat. *PLoS One* 6: e24462

812 Silvotti L, Cavaliere RM, Belletti S, Tirindelli R (2018) In-vivo activation of vomeronasal neurons
813 shows adaptive responses to pheromonal stimuli. *Sci Rep* 8: 8490

814 Silvotti L, Moiani A, Gatti R, Tirindelli R (2007) Combinatorial co-expression of pheromone
815 receptors, V2Rs. *J Neurochem* 103: 1753–1763

816 Sowa ST, Moilanen A, Biterova E, Saaranen MJ, Lehtio L, Ruddock LW (2021) High-resolution
817 Crystal Structure of Human pERp1, A Saposin-like Protein Involved in IgA, IgM and Integrin
818 Maturation in the Endoplasmic Reticulum. *J Mol Biol* 433: 166826

819 Stowers L, Holy TE, Meister M, Dulac C, Koentges G (2002) Loss of sex discrimination and male-
820 male aggression in mice deficient for TRP2. *Science* 295: 1493–1500

821 Takahashi K, Shibata T, Akashi-Takamura S, Kiyokawa T, Wakabayashi Y, Tanimura N, Kobayashi
822 T, Matsumoto F, Fukui R, Kouro T *et al* (2007) A protein associated with Toll-like receptor (TLR) 4
823 (PRAT4A) is required for TLR-dependent immune responses. *J Exp Med* 204: 2963–2976

824 Tanaka M, Treloar H, Kalb RG, Greer CA, Strittmatter SM (1999) G(o) protein-dependent survival
825 of primary accessory olfactory neurons. *Proc Natl Acad Sci U S A* 96: 14106–14111

826 Teufel F, Almagro Armenteros JJ, Johansen AR, Gislason MH, Pihl SI, Tsirigos KD, Winther O,
827 Brunak S, von Heijne G, Nielsen H (2022) SignalP 6.0 predicts all five types of signal peptides
828 using protein language models. *Nat Biotechnol* 40: 1023–1025

829 van Anken E, Pena F, Hafkemeijer N, Christis C, Romijn EP, Grauschopf U, Oorschot VM, Pertel
830 T, Engels S, Ora A *et al* (2009) Efficient IgM assembly and secretion require the plasma cell
831 induced endoplasmic reticulum protein pERp1. *Proc Natl Acad Sci U S A* 106: 17019–17024

832 Wakabayashi Y, Kobayashi M, Akashi-Takamura S, Tanimura N, Konno K, Takahashi K, Ishii T,
833 Mizutani T, Iba H, Kouro T *et al* (2006) A protein associated with toll-like receptor 4 (PRAT4A)
834 regulates cell surface expression of TLR4. *J Immunol* 177: 1772–1779

835 Werner T, Sweetman G, Savitski MF, Mathieson T, Bantscheff M, Savitski MM (2014) Ion
836 coalescence of neutron encoded TMT 10-plex reporter ions. *Anal Chem* 86: 3594–3601

837 Xiong E, Li Y, Min Q, Cui C, Liu J, Hong R, Lai N, Wang Y, Sun J, Matsumoto R *et al* (2019) MZB1
838 promotes the secretion of J-chain-containing dimeric IgA and is critical for the suppression of
839 gut inflammation. *Proc Natl Acad Sci U S A* 116: 13480–13489

840 Young JM, Trask BJ (2007) V2R gene families degenerated in primates, dog and cow, but
841 expanded in opossum. *Trends Genet* 23: 212–215
842

Figure 1

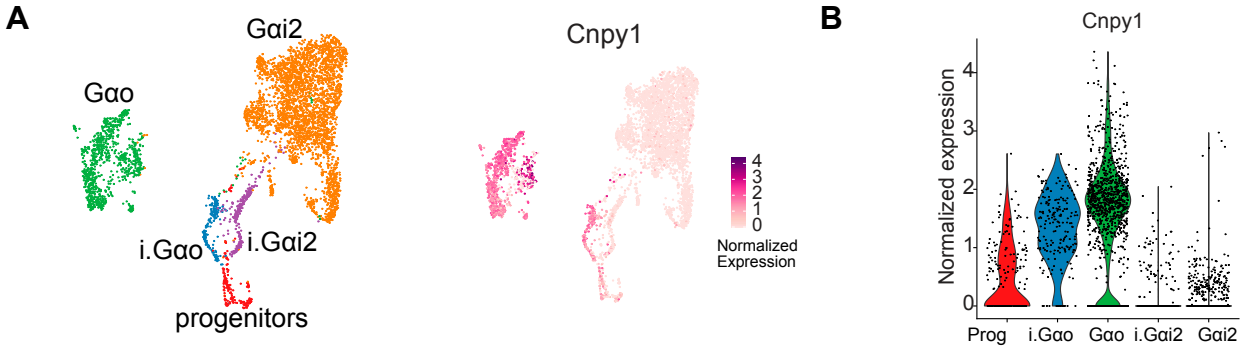

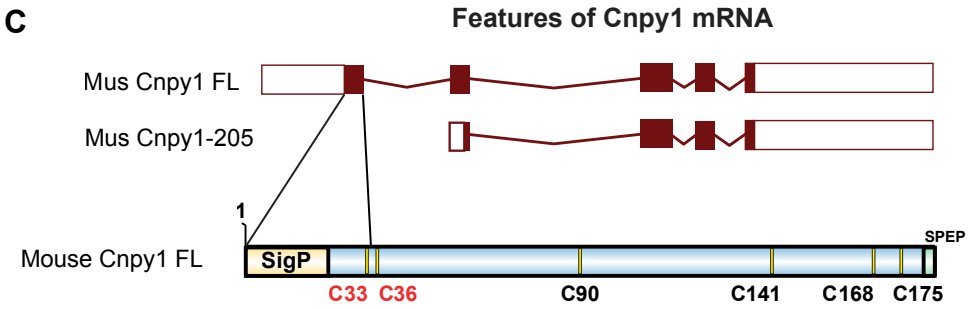

D

```
Cnpy1   1 ------------MGLALVPMALMILPA--LLLWP-----------------ILANDSEEPNVRCGACRALMDEVEYD  46
Cnpy2   1 ------------MKGWGWLALLL----G--VLLG--------------------TAWARRSQDLHCGACRALVDELEWE  41
Cnpy3   1 MESMSELAPRCLLFPLLLLLPLLLLPAP--KLGPSP-----------AGAEETDWVRL--PSKCEVCKYVAVELKSA  62
Cnpy4   1 -----MCGLRFIMGPVRLEILLFILAAY--GAWAEA-----------TKEEEDDTERL--PSKCEVCKLLSMELQEA  57
Cnpy5   1 ---------------MRLPLPLLLLFGCRAILGSAGDRVSLSASAPTLDDEEKYSAHMPAHLRCDACRAVAFQMGQR  62

Cnpy1  47 ITKARQK-KTKVGSYRIRPDGTQERKKVPLAQSEAFLIDLLDKVCMRM-NDYQLEDDPVTKQKYFRRYA-------- 113
Cnpy2  42 IARVDPKKTIQMGSFRINPDGSQSVVEVPYARSEAHLTELLEEVCDRM-KEYGEQIDPSTHRKNYVRVV-------- 109
Cnpy3  63 FEETGKTKEVIDTGYGIL--DGKG-SGVKYTKSDLRLIEVTETICKRL-LDYSLHKERTGSNRFAKGMSETFETLHN 135
Cnpy4  58 LSRTGRSREVLELGQVLD--TGKRKRHVPYSLSETRLEEALENLCERI-LDYNVHAERKGSLRYAKGQSQTMATLKG 131
Cnpy5  63 LAKAEAKSHTP------DASGLQE-------LSESTYTDVLDQTCSQNWQSYGVHEVNQMKR--LTGPG-------- 116

Cnpy1 114 -PRKGDKIYKEYKKFFFYSD--AFRPL---------KFACEAII-EKYEDEIFELIAQEAN-HLADMLCNEKSDL-- 174
Cnpy2 110 -SRNGESSELDLQGIRIDSD--ISGTL---------KFACESIV-EEYEDELIEFFSREAD-NVKDKLCSKRTDL-- 170
Cnpy3 136 LVHKGVKVVMDIPYELWNETSAEVADLK---------KQCDVLV-EEFEEVIEDWYRNHQEEDLTEFLCANHVLKGK 202
Cnpy4 132 LVQKGVKVDLGIPLELWDEPSVEVTFLKKQVRIPVPTSQCETML-EEFEDVVGDWYFHHQEQPLQHFLCERHVLPAS 207
Cnpy5 117 -LSKGPEP--RISVMISGGP--WPNRL---------SKTCFHYLGEFGEDQIYEAYRQGQA-NLEALLCGGTHGP-- 176

Cnpy1 175 ---CGTPTNSPEP------------------------------------------------------------------ 184
Cnpy2 171 ---CDHALHRSHDEL------------------------------------------------------------------ 182
Cnpy3 203 DTSCLAERWSGKKGDIASLGGKKSKKKRSGVKGSSSGSSKQRKELGGLGEDANAEEEEGVQKASPLPHSPPDEL 276
Cnpy4 208 ETACLREAWTGKEKISDGQEEA-----------------------------DDEEEEEEEEITKTSGNPKHDPEDL 254
Cnpy5 177 ---CSQEILAQREEL------------------------------------------------------------------ 188
```

Figure 1. Description of the complete mouse Cnpy1 gene.
A) UMAP (left, from Devakinandan et. al. 2024) and feature plot (right) showing *Cnpy1* gene expression amongst vomeronasal sensory neuron clusters coded in different colors corresponding to progenitors (prog), immature Gαo (i.Gαo), immature Gαi2 (i.Gαi2), mature Gαo (Gαo), mature Gαi2 neurons (Gαi2). *Cnpy1* expression is restricted to immature and mature Gαo neurons. **B**) Violin plot shows the distribution and extent of *Cnpy1* expression in neuronal clusters. **C**) Schematic showing the transcript structure of full length *Cnpy1* (Cnpy1-FL) and its comparison with transcript from Ensembl database (Cnpy1-205, ENSMUST00000141601). Exons are represented as boxes, with coding regions shaded and untranslated region as hollow boxes. The first exon in Cnpy1-FL contributes an upstream translation initiation site for a longer ORF with a signal peptide (SigP, **Figure S1**) and two out of the six signature cysteine residues comprising saposin-like domain. **D**) Alignment of Cnpy1 (Cnpy1-FL) with Cnpy2-5 mouse protein sequences showing conserved 6-cysteine signature highlighted in yellow. Putative signal sequence in the N-terminal region of Cnpy1-FL is highlighted in red.

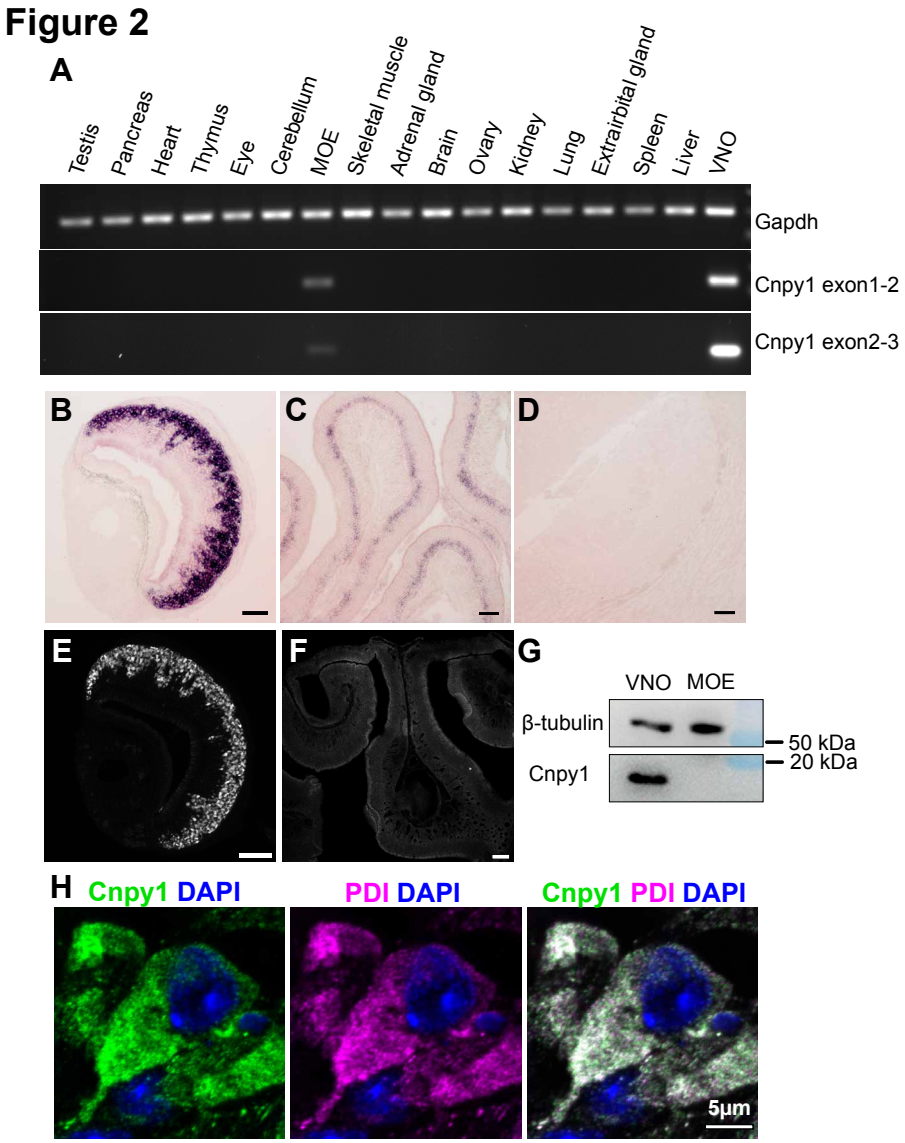

Figure 2. Cnpy1 is a Gαo VNO neuron specific ER protein.
A) PCR amplification with primers specific to *Cnpy1* exon1-2 (Cnpy1-FL) or exon2-3 (common to Cnpy1-FL and Cnpy1-205) using cDNA from various mouse tissues as a template. Amplification from both primer sets visualized by agarose gel electrophoresis, shows a bright band in the vomeronasal organ (VNO) and a weaker band in the main olfactory epithelium (MOE), with Glyceraldehyde-3-phosphate dehydrogenase (*Gapdh*) amplification as a control for cDNA integrity. **B-D**) RNA in-situ hybridization with anti-sense *Cnpy1* ribo-probe shows strong signal in VNO coronal sections (**B**), lower in MOE (**C**), and no expression in accessory olfactory bulb (**D**). **E, F**) Anti-Cnpy1 custom antibody immunofluorescence shows protein expression specifically within VNO basal neurons (**E**), but not in MOE (**F**). **G**) Western blot shows Cnpy1 band in VNO but not MOE lysate, with β-tubulin as a loading control. **H**) High magnification image of sensory neurons from VNO coronal section labelled with anti-Cnpy1 (green), anti-PDI (magenta) as endoplasmic reticulum (ER) marker, and DAPI (blue) marking the nucleus. Cnpy1 is co-localized in the ER. **B-F** scale bar is 100 μm.

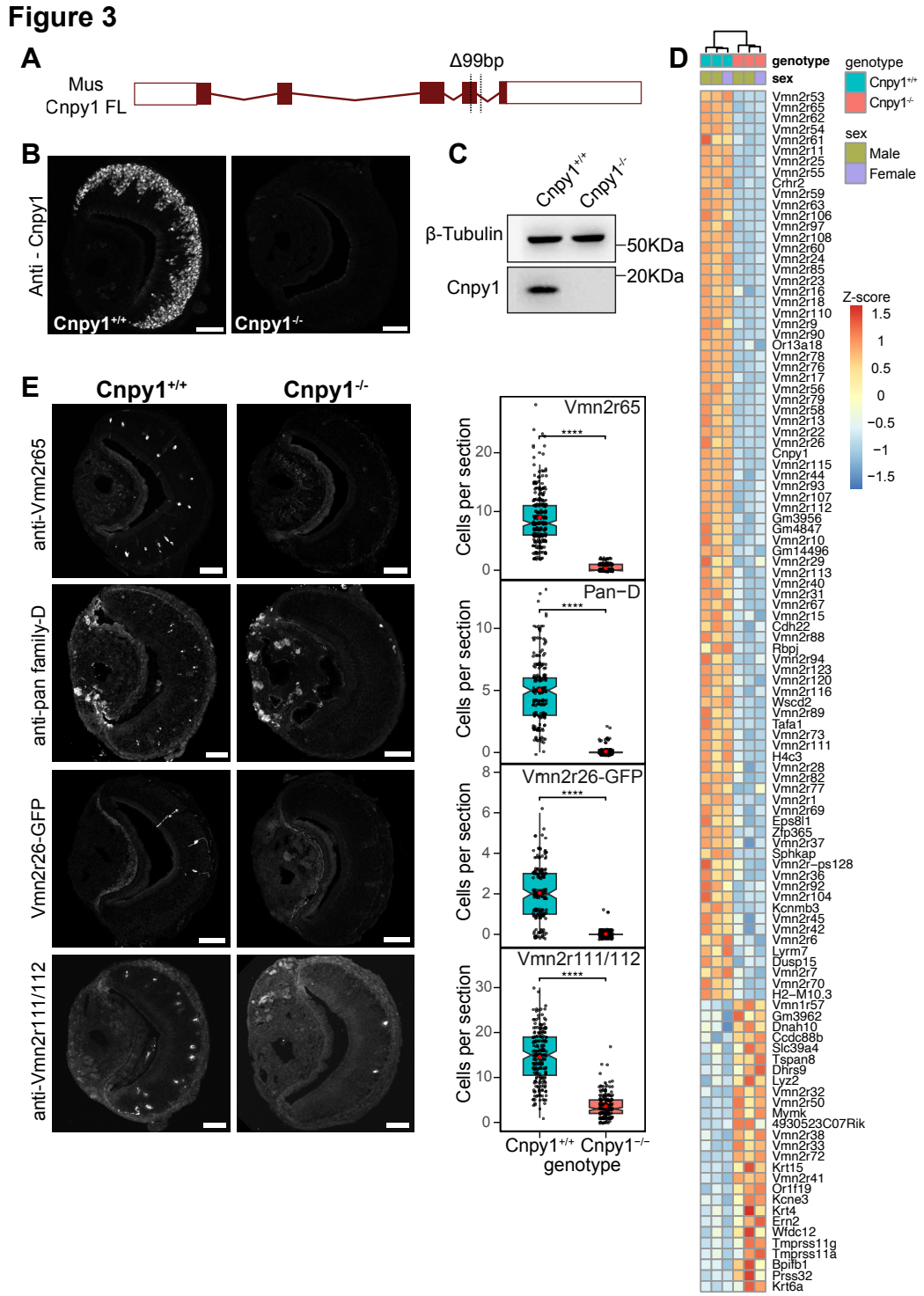

Figure 3. Deletion of Cnpy1 results in downregulation of multiple V2Rs

A) Schematic of Cnpy1 gene showing 99 base pair deletion in exon-4 leading to generation of a Cnpy1$^{-/-}$ mouse line. **B, C**) Absence of Cnpy1 protein confirmed by anti-Cnpy1 immunofluorescence labeling of VNO section (**B**) and western blot (**C**), with β-tubulin as loading control. **D**) Heatmap of differentially expressed genes from bulk RNA sequencing performed on Cnpy1$^{-/-}$, Cnpy1$^{+/+}$ littermate mouse (3 each) VNOs. 111 genes with adjusted p-value < 0.01 and absolute fold change of 1.5 are shown ordered by fold change (most downregulated genes on the top). Of the 84 downregulated genes, 66 code for V2R (Vmn2r) GPCRs. **E**) Immunolabeling of p60 VNO sections with antibodies against Vmn2r65, pan-family D V2Rs, Vmn2r111/112 and GFP neurons representing Vmn2r26 shows absence of these V2R expressing neurons in Cnpy1$^{-/-}$ VNOs compared to Cnpy1$^{+/+}$. Representative images are on the left; box plots on the right show quantification of cells per section from at least 50 sections for each of 3 replicates per genotype. The notch on the box plots indicates the median and red dot denotes mean. Mann–Whitney U test was performed to measure statistical significance, **** indicates p value < 10^{-4}. Scale bar: 100 µm.

Figure 4

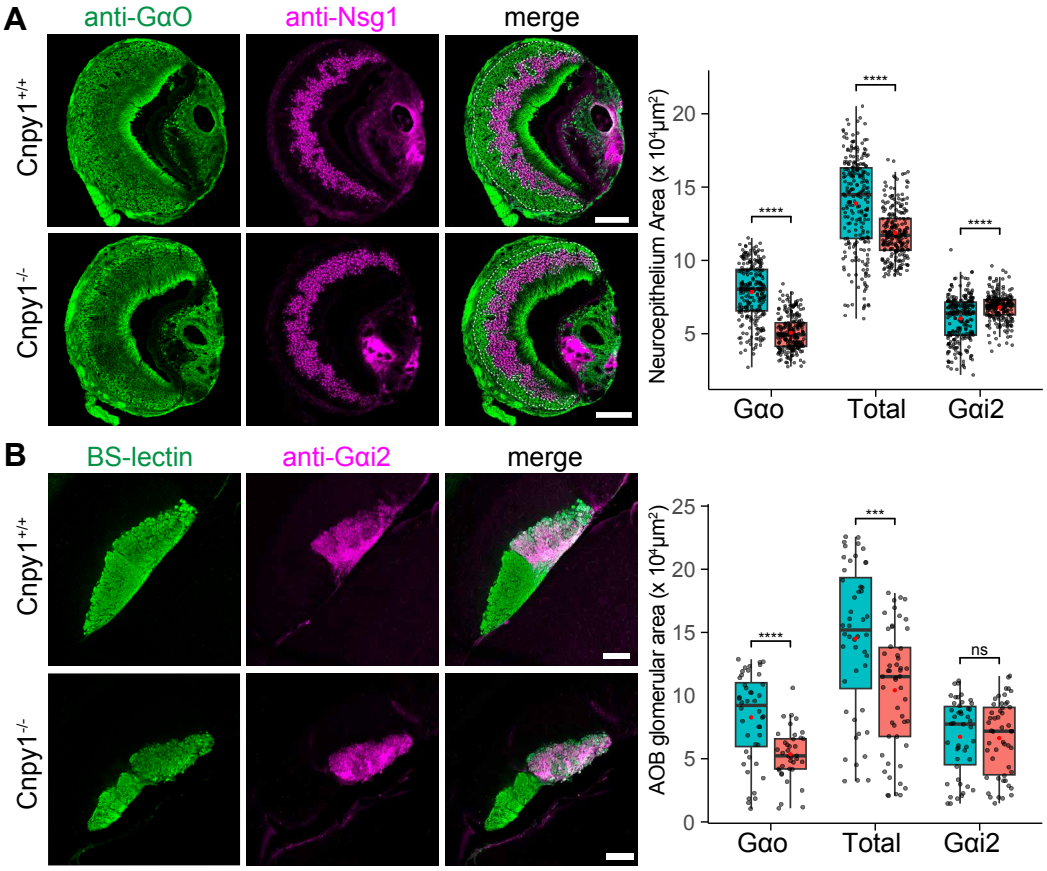

Figure 4. Gαo zone is reduced in Cnpy1$^{-/-}$ mice.
A) VNO cryosections from p60 Cnpy1$^{-/-}$ or Cnpy1$^{+/+}$ mice immunolabelled to mark Gαo or Gαi2 zones (anti-Nsg1/Neep21). Representative images (left) show the area (dotted line) that was quantified (right) from 3 pairs of littermate mice (Cnpy1$^{+/+}$- 244 and Cnpy1$^{-/-}$ - 238 sections). **B**) Representative images (left) of AOB vibratome sections co-labelled with BS-lectin that marks the combined glomerular and nerve layer area along with anti-Gαi2, followed by their quantification (3 animals, Cnpy1$^{+/+}$- 44 and Cnpy1$^{-/-}$ - 37 sections) on the right. Gαo area was quantified by subtracting Gαi2 from the total area. Both VNO and AOB quantifications show a substantial reduction in Gαo area, which results in a thinning of the total neuroepithelium. There is no reduction in the Gαi2 area. Horizontal line on the box plots indicates the median and red dot denotes mean. Mann–Whitney U test was performed to measure statistical significance. **** - p value < 10^{-4}; *** - p value < 10^{-3}; ns - not significant. Scale bar: 100 µm.

Figure 5

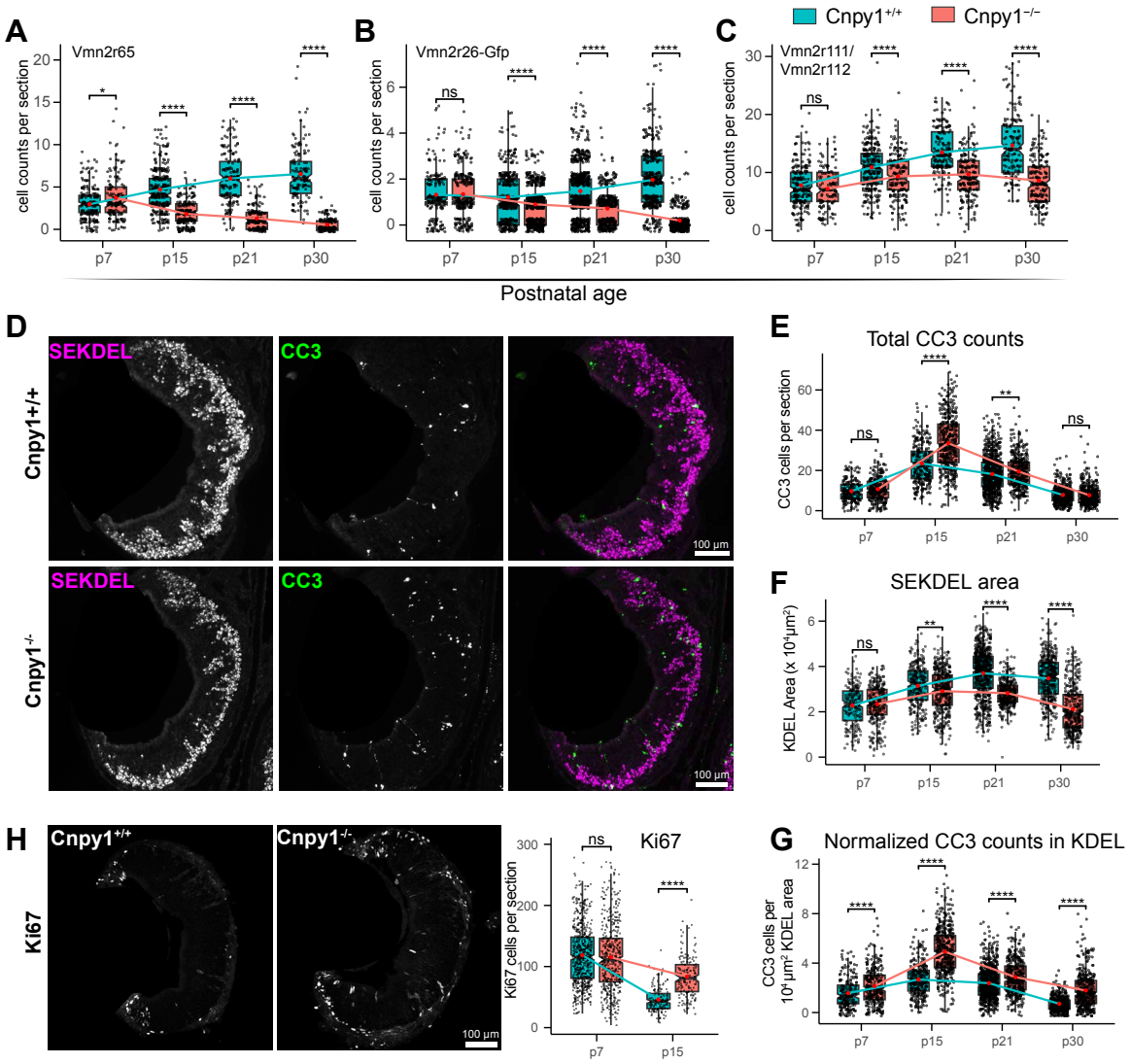

Figure 5. Enhanced cell death and neurogenesis in Cnpy1$^{-/-}$ VNO neuroepithelium.
A-C) Quantification of V2R expressing neurons from VNO cryosections of Cnpy1$^{-/-}$ or Cnpy1$^{+/+}$ mice across postnatal age, was performed using anti-V2R antibodies shown in **Figure 3**. Counts of Vmn2r65 (**A**), Vmn2r26 (**B**), Vmn2r111/112 (**C**) are comparable between Cnpy1$^{-/-}$ or Cnpy1$^{+/+}$ at p7. In Cnpy1$^{+/+}$ number of neurons expressing these V2Rs increase with postnatal development, but in Cnpy1$^{-/-}$ VNOs they decline from p15 onwards. **D-G**) Representative images of p15 VNO cryosections labelled with anti-SEKDEL to mark Gαo zone, along with Cleaved Caspase-3 (CC3), a marker of apoptotic cells. CC3 positive cells quantified in the neuroepithelium (**E**) show an increase in p15 Cnpy1$^{-/-}$ VNO. The Gαo zone (SEKDEL) area in Cnpy1$^{-/-}$ and Cnpy1$^{+/+}$ VNOs is comparable at p7 but declines from p15 onwards (**F**). The total number of CC3 cells overlapping with the Gαo area as well as CC3 numbers normalized to the declining Gαo area at respective age groups (**G**), show elevated Gαo zone specific apoptosis across postnatal ages, with a peak at p15 in Cnpy1$^{-/-}$. **H**) Labeling and quantification of VNO sections with anti-Ki67 indicates elevated levels of neurogenesis at p15 age in Cnpy1$^{-/-}$ VNO compared to Cnpy1$^{+/+}$. All quantifications were performed with 5 animals at each age, genotype and across at least 150 sections. Notch on the box plots indicates the median and red dot denotes mean. Mann–Whitney U test was performed to measure statistical significance. **** - pvalue < 10^{-4}; *** - p value < 10^{-3}; ** p value < 10^{-2}; * - p value < 0.05; ns - not significant.

Figure 6

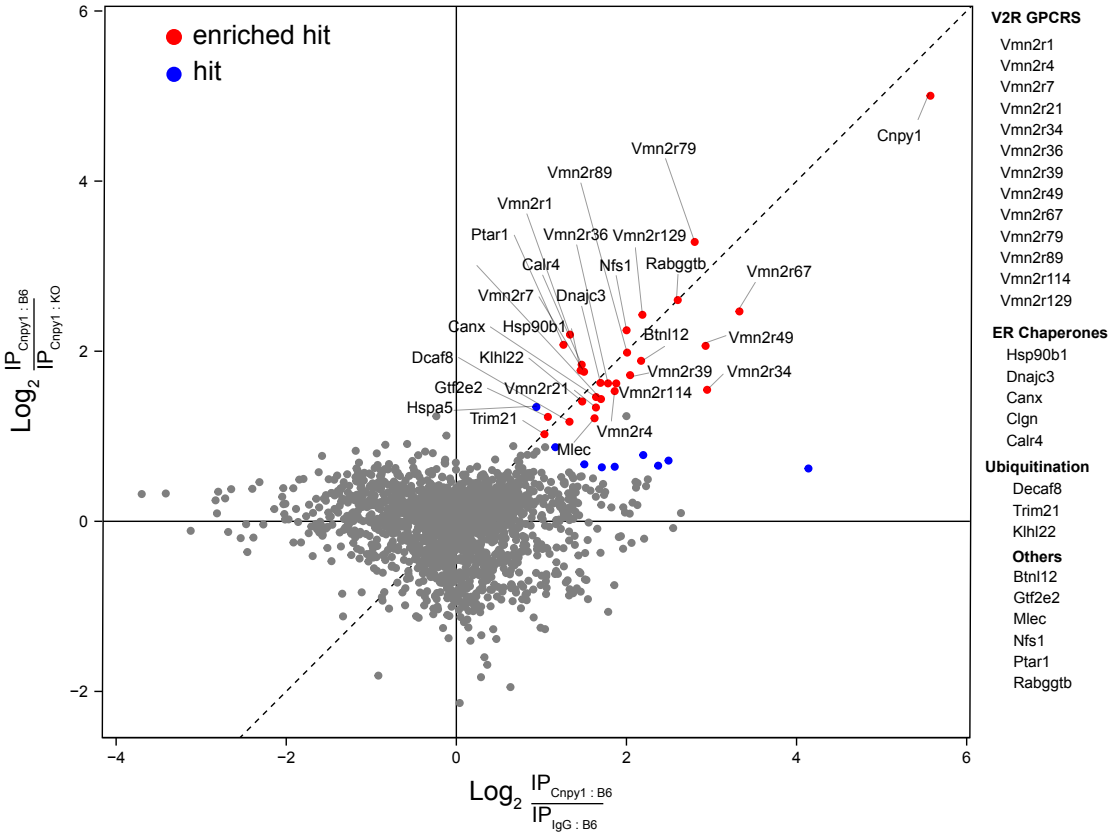

Figure 6. Cnpy1 interacts with Vmn2r GPCRs and ER chaperones.
Immuno-precipitation (IP) of Cnpy1 followed by quantitative mass-spectrometry to identify specific interacting partners of Cnpy1 from mouse VNO. Cnpy1 IP performed using anti-Cnpy1 from C56Bl/6 (B6) mouse VNO lysates ($IP_{Cnpy1:B6}$) was compared with negative control IPs consisting of normal rabbit IgG ($IP_{IgG:B6}$) and anti-Cnpy1 IP from Cnpy1$^{-/-}$ (knockout -KO) mouse VNO lysate ($IP_{Cnpy1:KO}$). Each IP was performed with 3 biological replicates, pooling VNOs from 50 mice per replicate, except for $IP_{IgG:B6}$ which was performed in duplicate. Specific hits are identified by comparing fold change of signal intensity from [$IP_{Cnpy1:B6}$ over $IP_{Cnpy1:KO}$] (Y axis) and [$IP_{Cnpy1:B6}$ over $IP_{IgG:B6}$] on X axis. Proteins with an absolute fold change of 2 or more and a false discovery rate less than 0.05 in both comparisons (X and Y axes) falling along the diagonal are considered specific interacting proteins (enriched hits) from both comparisons and are marked in red. A list of enriched hits is provided on the right. Hits with a false discovery rate < 0.05, showing an absolute fold change > 2 in one comparison and between 1.5 and 2 in the other, are highlighted in blue.

Figure 7

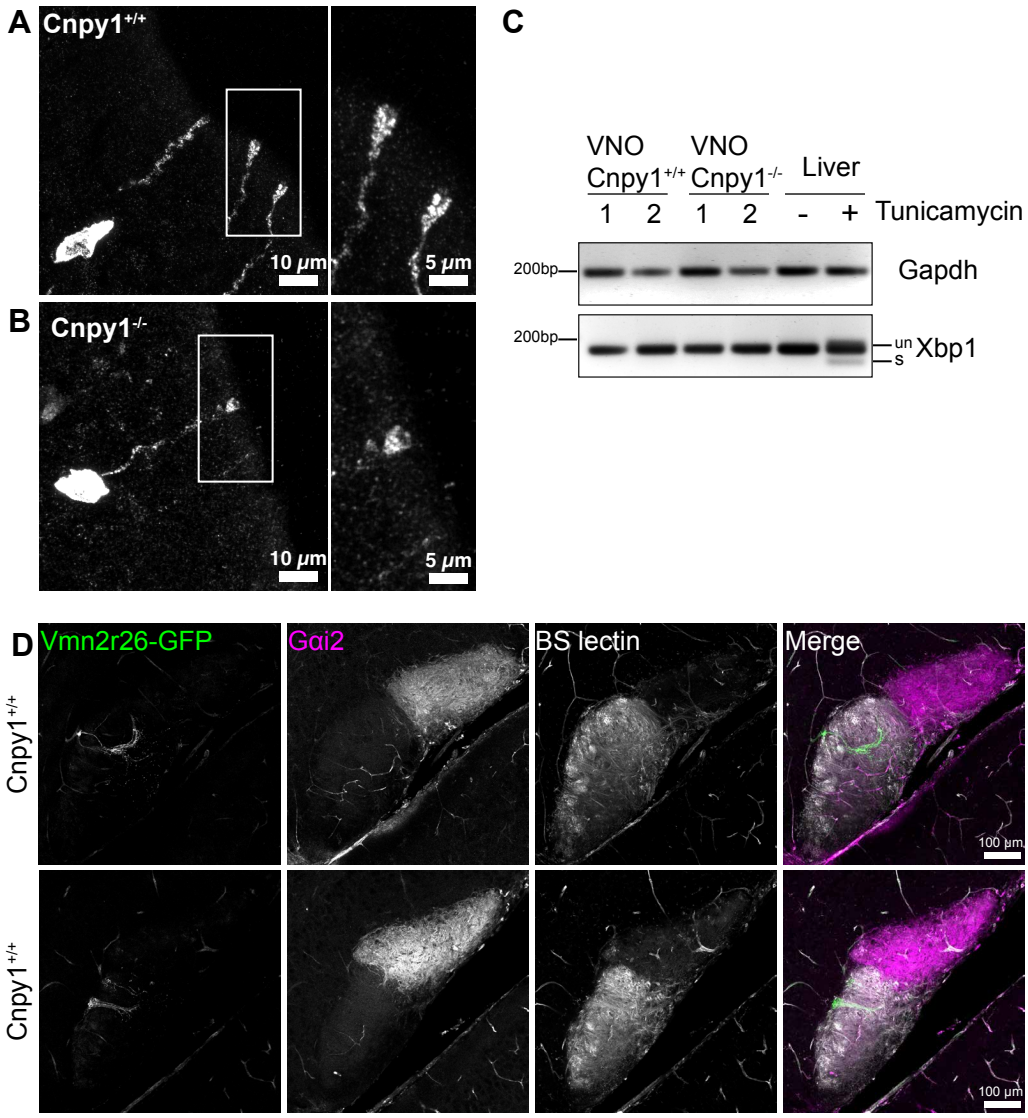

Figure 7. Cnpy1 deficiency preserves V2R localization, glomerular projections and does not activate *Xbp1* splicing.

A, B) Immunofluorescence confocal microscopy images of anti-Vmn2r65 labeling on p15 Cnpy1$^{+/+}$ and Cnpy1$^{-/-}$ VNO, show comparable GPCR localization to dendritic tips in both genotypes. **C**) PCR of *Xbp1* from two replicates each of Cnpy1$^{+/+}$ and Cnpy1$^{-/-}$ p15 VNO cDNA using primers spanning the splice site. *Xbp1* splicing is not seen in both genotypes. cDNA from Tunicamycin treated mouse liver, used a positive control, shows spliced (s) and unspliced (un) *Xbp1* bands, indicative of unfolded protein response. Size (basepairs) of the nearest DNA marker band is marked on the left. *Gapdh* was used a control for cDNA integrity. **D**) Representative immunofluorescence confocal microscopy images detect axonal projections from Vmn2r26-IRES-GFP neurons to the glomerular regions of the accessory olfactory bulb (AOB) in p7 Cnpy1$^{+/+}$ and Cnpy1$^{-/-}$ mice. Targeting and coalescence of GFP labeled projections to glomeruli within the posterior part of the AOB appears to be intact in both.

Figure 8

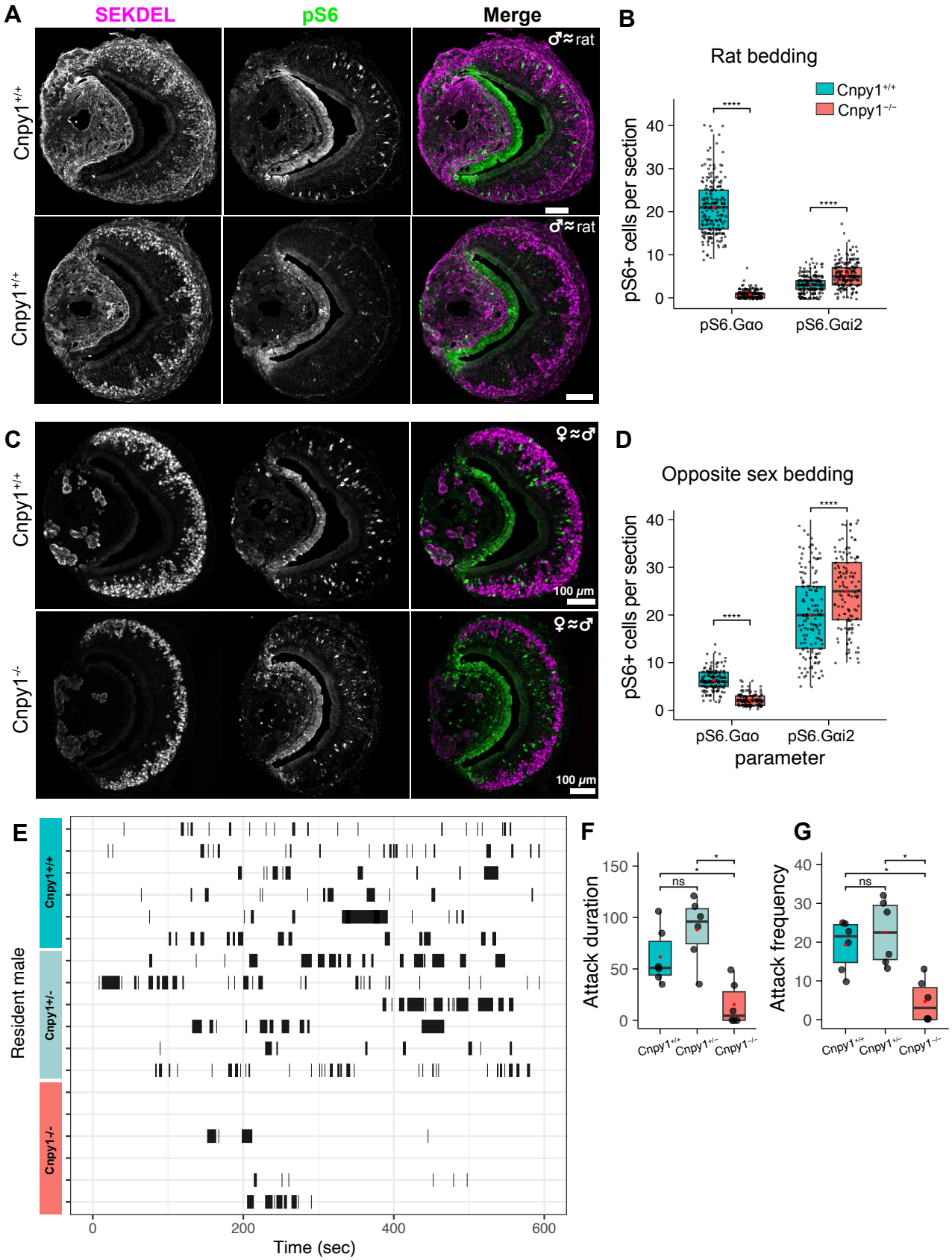

Figure 8. Impaired Gαo neuron activation and behavior in Cnpy1$^{-/-}$ mice.
Representative images and quantification of activated neurons from VNO sections obtained from p60 Cnpy1$^{-/-}$ or Cnpy1$^{+/+}$ mice after exposure to rat bedding (predator signal) (**A,B**) or opposite sex bedding (**C, D**). In both sets, activated VSNs are detected by anti-pS6 (green) and sections are co-labelled with anti-SEKDEL (magenta) to mark Gαo zone neurons. Quantification of pS6+ cells from 3 biological replicates and at least 50 sections per mouse (**B, D**), shows substantially reduced activation of Cnpy1$^{-/-}$ Gαo neurons compared to Cnpy1$^{+/+}$. A small but significant increase in activated neurons outside Gαo zone (Gαi2) is also detected. **E**) Raster plot showing attack events by a male resident mouse towards intruder mouse over time. The duration of attacks (**F**) as well as number of attacks (**G**) from six resident animals each from Cnpy1$^{+/+}$, Cnpy1$^{+/-}$ and Cnpy1$^{-/-}$ is shown as box plots. Red dot on the box plots represents the mean. Cnpy1$^{-/-}$ male mice show far fewer attacks compared to mice having an intact copy of Cnpy1 gene. Mann–Whitney U test was performed to measure statistical significance. **** - p value < 10^{-4}; * - p value < 0.05 and ns - not significant.

Supplementary Figure S1

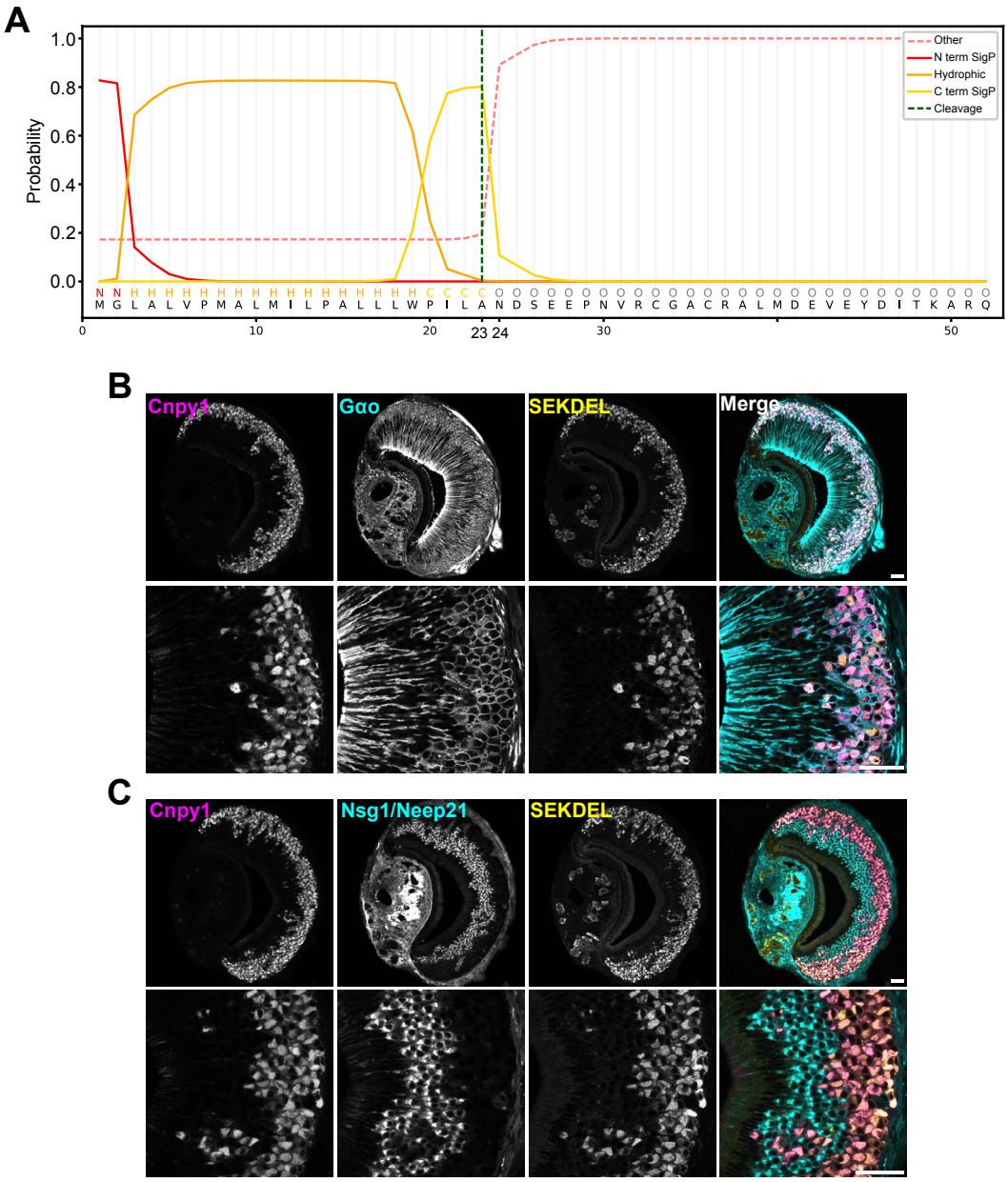

Figure S1. Cnpy1 is expressed in Gαo neurons.
A) Cnpy1 N-terminal signal sequence predicted by SignalP 6.0 with cleavage site between amino acids 23-24 of mouse Cnpy1-FL. **B**) Immunofluorescence confocal microscopy images of VNO sections labelled with anti-Cnpy1, anti-Gαo, anti-SEKDEL; show SEKDEL and Cnpy1 co-localization within Gαo neurons. **C**) Images of VNO section labelled with anti-Cnpy1, anti-Nsg1/Neep21 (marker for Gαi2 neurons), anti-SEKDEL confirms the exclusive expression of Cnpy1 in Gαo neurons. Scale bar: 50μm.

Supplementary Figure S2

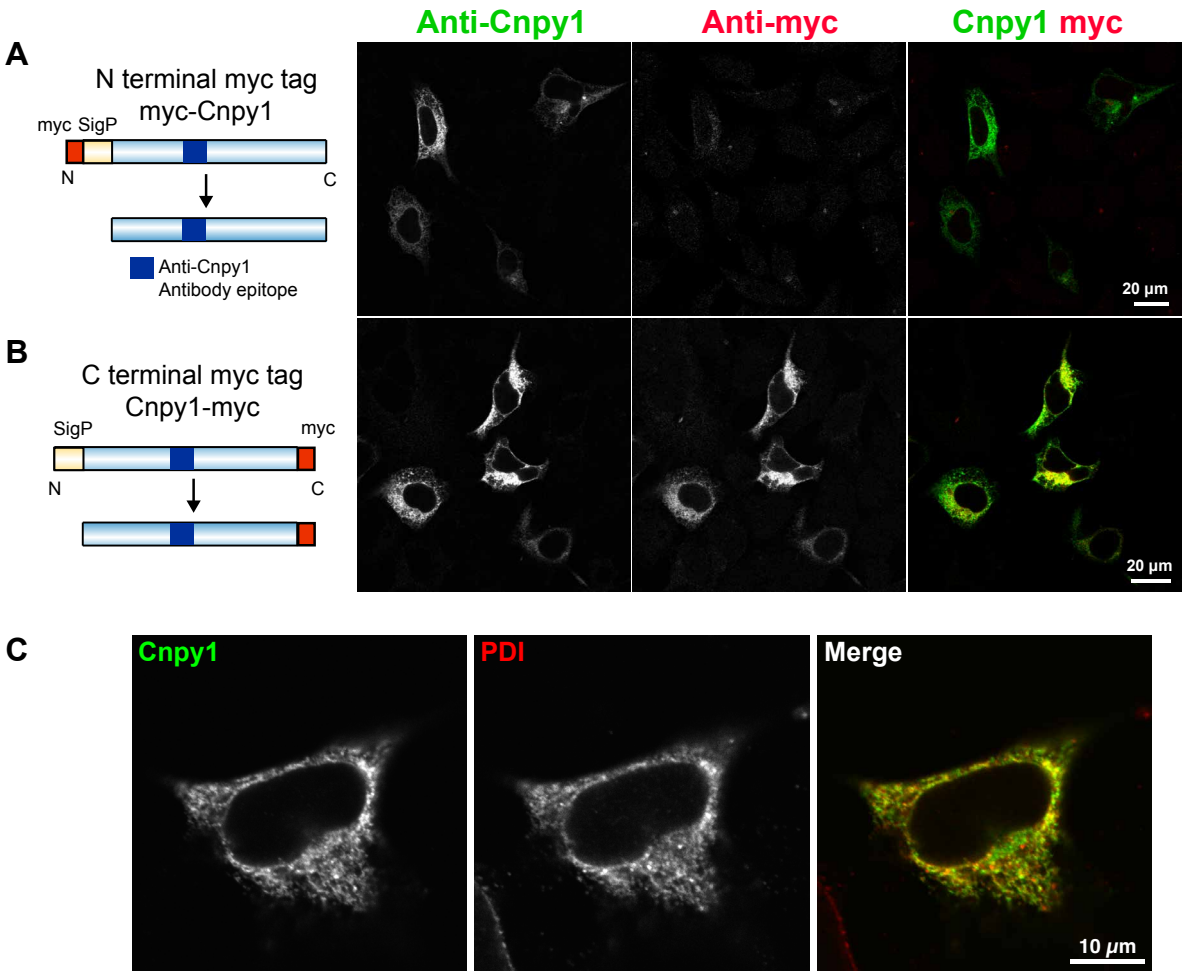

Figure S2. Expression of mouse Cnpy1 in HEK293 cells.
A,B) Cnpy1-FL cloned with N-terminal myc tag (myc-Cnpy1) (**A**), or C-terminal myc tag (Cnpy1-myc) (**B**), were transiently expressed in HEK293 cells and immunolabeled with anti-Cnpy1, anti-myc tag. The schematic on the left shows the position of myc with respect to signal peptide (SigP) and location of Cnpy1 antibody binding epitope. Anti-Cnpy1 detects the expression of both constructs, whereas anti-myc signal is seen only with Cnpy1-myc, confirming the cleavage of N-terminal signal peptide. **C**) Immunolabeling of transiently expressed Cnpy1 and an ER resident protein – PDI shows ER localization in HEK293 cells.

Supplementary Figure S3

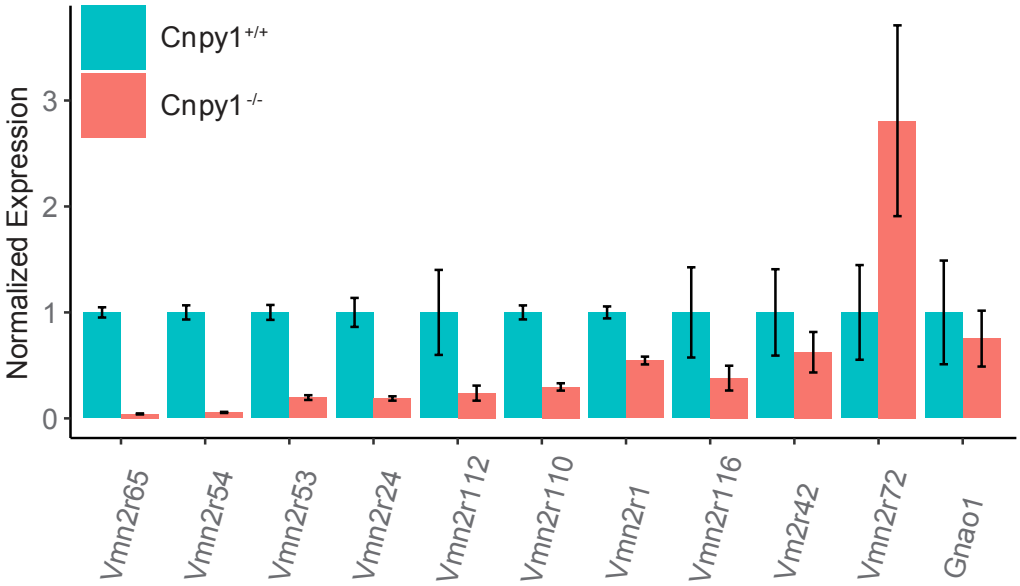

Figure S3. Q-PCR validation of V2R RNA levels from Cnpy1$^{-/-}$ and Cnpy1$^{+/+}$ VNO. Validation of differences observed in Cnpy1$^{-/-}$ and Cnpy1$^{+/+}$ VNO bulk RNA sequencing using Taqman probes specific for selected Vmn2r genes. Expression level of each gene relative to Cnpy1$^{+/+}$ is represented as mean and error bars represent standard error.

Supplementary Figure S4

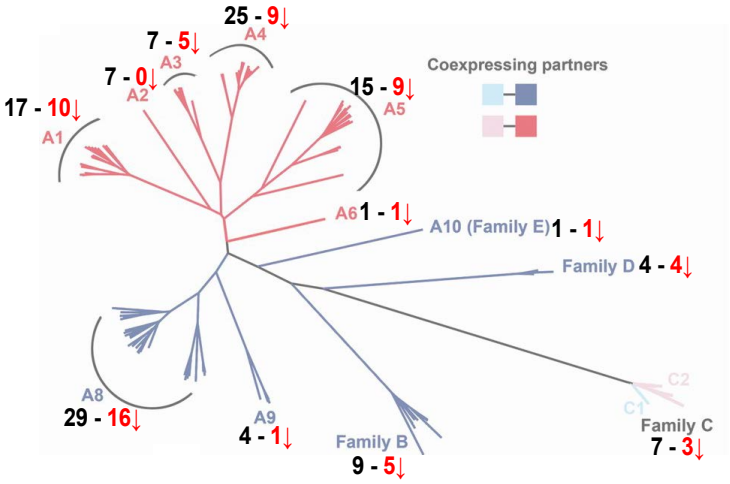

Figure S4. V2R downregulation in Cnpy1 knockout is not family-specific.
Phylogenetic tree adapted from Francia et al., 2014 (licensed under CC BY), showing classification of V2Rs into families based on sequence homology. The number of downregulated V2Rs corresponding to **Figure 3D** is shown in red with a downward facing arrow, adjacent to the total count for each family. Downregulated V2Rs are distributed across all families.

Supplementary Figure S5

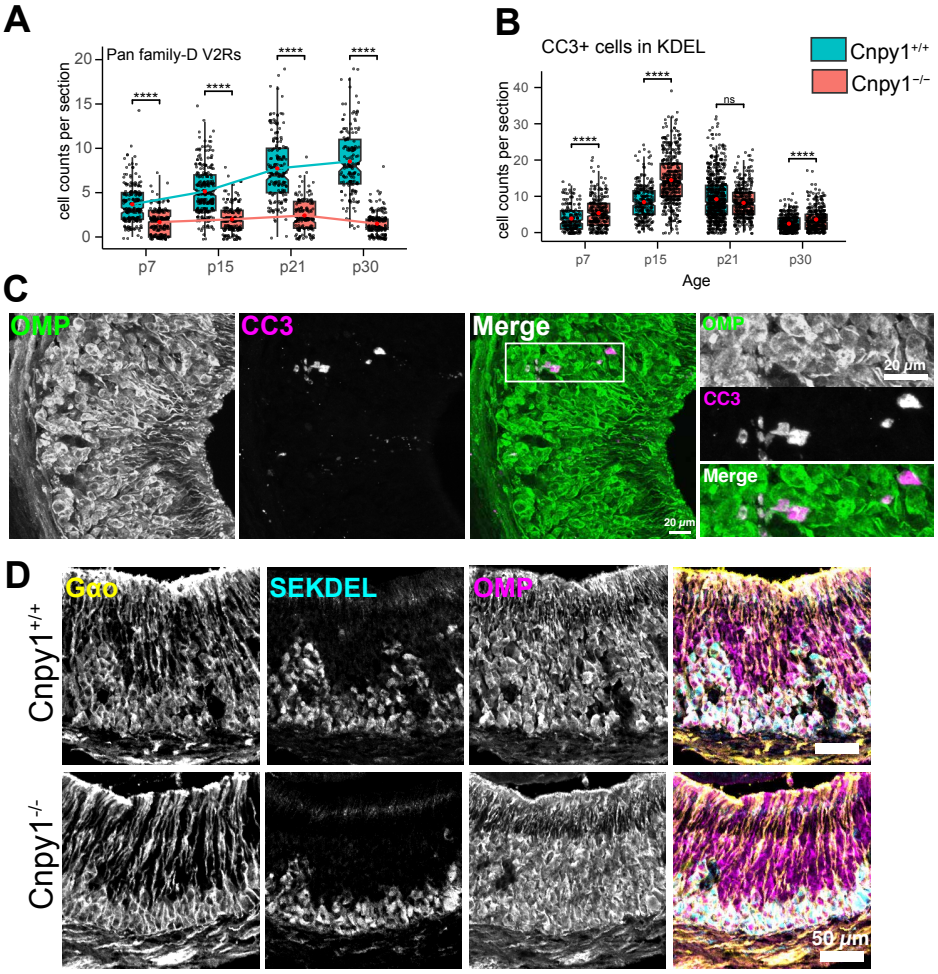

Figure S5

A) Cell counts per section from VNO sections across postnatal age labeled with anti-pan family-D V2Rs show progressive decline in Family-D expressing neurons during postnatal development of Cnpy1$^{-/-}$ mice. **B**) Total number of CC3 labelled cells overlapping with Gαo (anti-SEKDEL) zone per section, quantified across postnatal age. Mann–Whitney U test was performed to measure statistical significance. **** - p value < 10^{-4} and ns - not significant. **C**) Immunolabeling of OMP and CC3 on p15 Cnpy1$^{-/-}$ sections showing CC3+ apoptotic neurons are also labeled with OMP, a marker of mature neurons. **D**) Representative immuno-fluorescence confocal microscopy images of VNO sections from p60 mice, labelled with anti-Gαo, anti-SEKDEL and anti-OMP. Similar to Cnpy1$^{+/+}$ VNO, anti-SEKDEL is a marker for Cnpy1$^{-/-}$ Gαo neurons. Gαo neurons in Cnpy1$^{-/-}$ are also labelled with anti-OMP indicating their developmental status as mature neurons.

Supplementary Figure S6

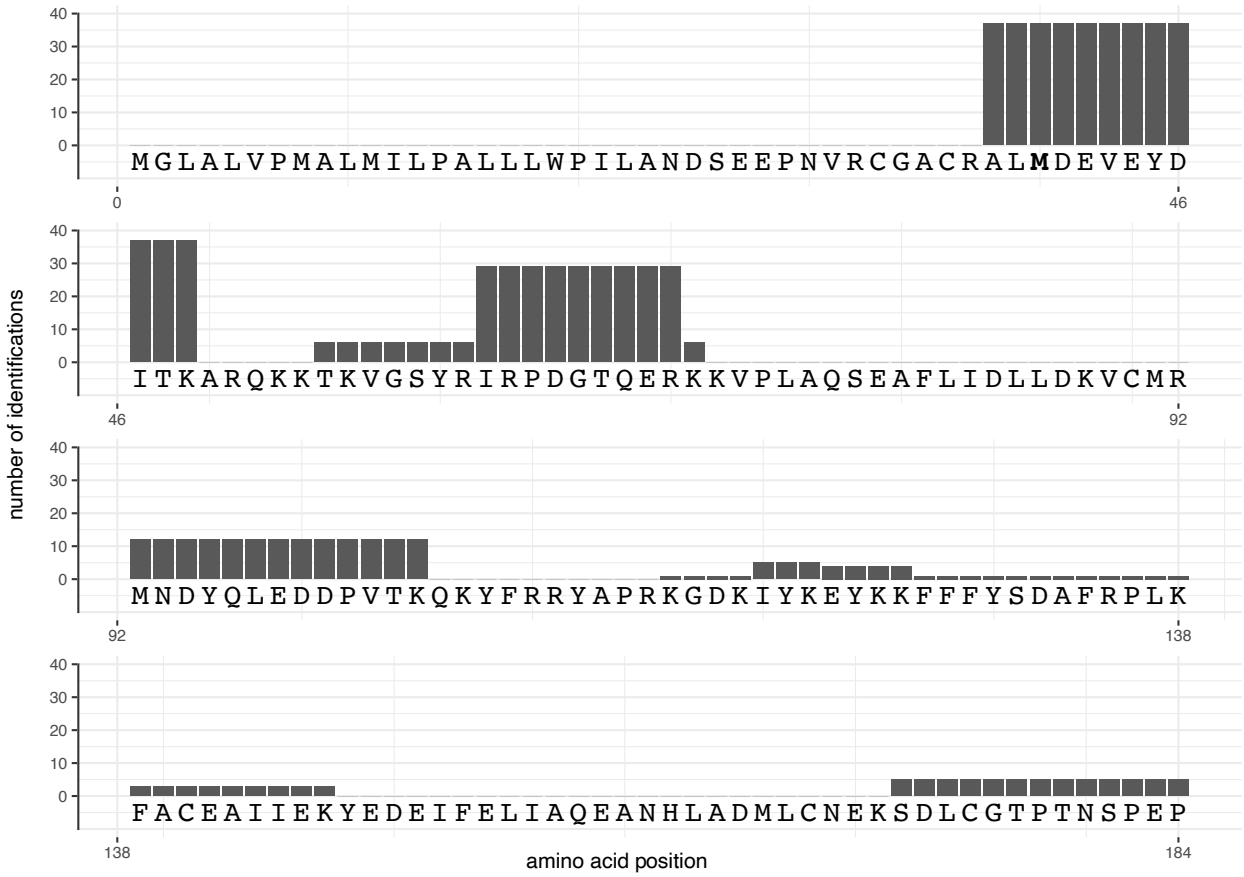

Figure S6
Alignment of Cnpy1 amino acid sequence with trypsin digested peptides detected by mass-spectrometry. Number of identifications for each peptide detected is marked on y-axis. Methione (M40) in bold is the translation start site for Ensembl transcript - ENSMUST00000141601. The presence of signal from peptide containing AL before M40 re-confirms the upstream translation start site.

Supplementary Figure S7

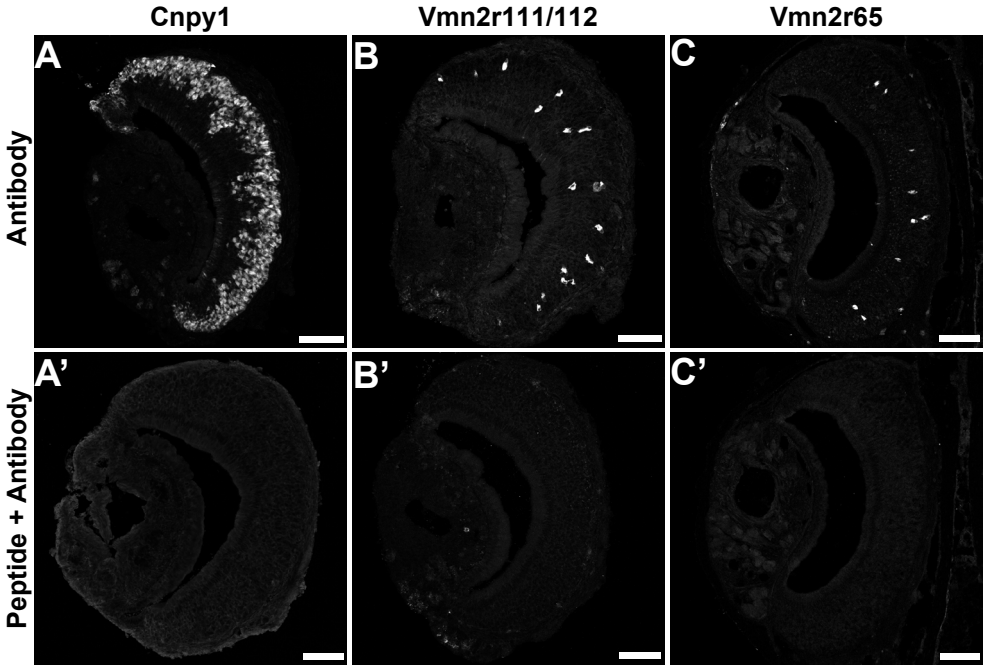

Figure S7. Generation of custom polyclonal antibodies.
Anti-Cnpy1, anti-Vmn2r111/112 and anti-Vmn2r65 antibodies generated by injecting KLH conjugated DDPVTKQKYFRRYAPRKGD, FWKMKRNENKDRNQ, and QKVNFTQKFSDTHSKIEYNH, respectively. Specific immunolabeling (**A-C**) with each antibody is blocked after pre-incubation of each antibody with the respective immunogenic peptide (**A'-C'**). Scale bar: 100 μm

Supplementary Figure S8

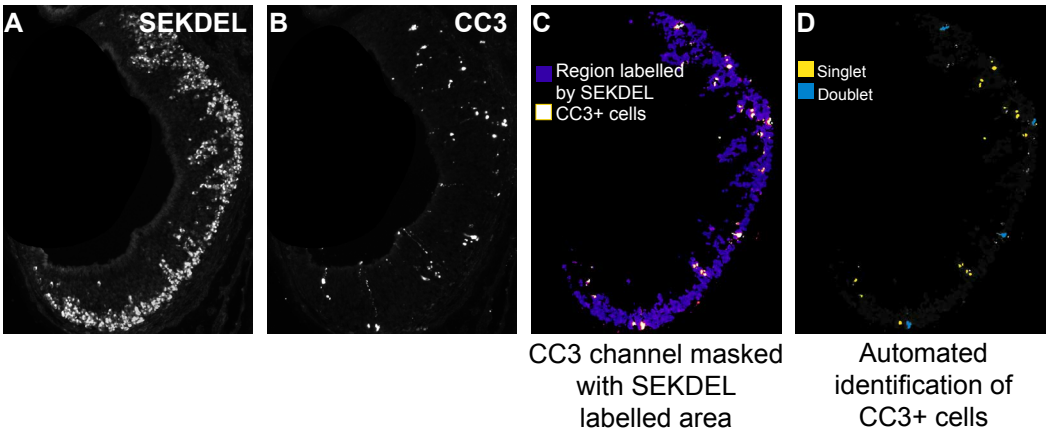

Figure S8. Automated quantification of cell numbers from images.
Immunofluorescence images were manually masked to remove the non-sensory epithelium from all channels (**A, B**). An *ilastik* segmentation model was trained to identify pixels labeled by anti-SEKDEL (**A**) and to generate a mask, which was then applied to the CC3 channel (**B**) to segement the SEKDEL-marked region in CC-3 channel (**C**). An independently trained object identification model was subsequently used to detect CC3-positive cells, classifying them as either singlets or doublets within the SEKDEL-segmented CC3 images (**D**).